Cell-cell metabolite exchange creates a pro-survival metabolic environment that extends lifespan

Cell

Article

Cell-cell metabolite exchange creates a pro-survival metabolic environment that extends lifespan

Graphical abstract

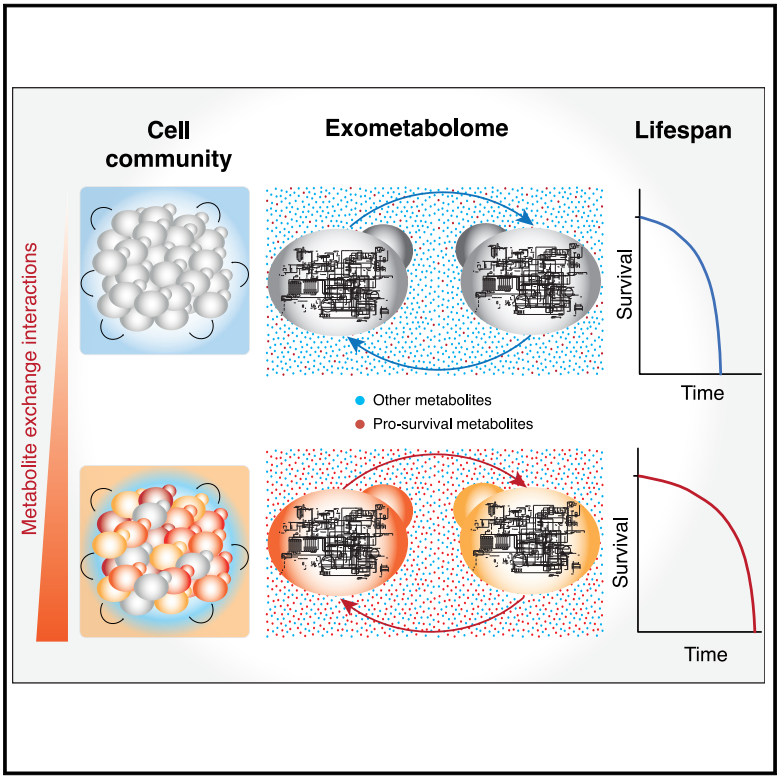

Authors

Clara Correia-Melo, Stephan Kamrad, Roland Tengölics, ..., Balázs Papp, Mohammad Tauqeer Alam, Markus Ralser

Correspondence

claramelo85@gmail.com (C.C.-M.), markus.ralser@charite.de (M.R.)

In brief

Communities in which cells interact for the biosynthesis of methionine enrich their extracellular space in protective metabolites, including glycerol, have increased activity of anti-aging processes, and show an extended lifespan.

Highlights

- Yeast cells exchange metabolites across generations
- Metabolite exchange interactions determine cellular lifespan
- Metabolic reconfigurations result in the export of protective metabolites
- Multiple pathways of aging are altered by a lifespan-extending exometabolome

Correia-Melo et al., 2023, Cell *186*, 63–79
January 5, 2023
https://doi.org/10.1016/j.cell.2022.12.007

CellPress

Cell

CellPress
OPEN ACCESS

Article

Cell-cell metabolite exchange creates a pro-survival metabolic environment that extends lifespan

Clara Correia-Melo,[1,2,3,*] Stephan Kamrad,[1] Roland Tengölics,[4,5] Christoph B. Messner,[1,6] Pauline Trebulle,[1,7] StJohn Townsend,[1,3] Sreejith Jayasree Varma,[3] Anja Freiwald,[3,8] Benjamin M. Heineike,[1,7,9,10] Kate Campbell,[2] Lucía Herrera-Dominguez,[1] Simran Kaur Aulakh,[1,7] Lukasz Szyrwiel,[1,3] Jason S.L. Yu,[1] Aleksej Zelezniak,[1,11,12,13] Vadim Demichev,[1,2,3] Michael Mülleder,[1,2,8] Balázs Papp,[4,5] Mohammad Tauqeer Alam,[14] and Markus Ralser[1,2,3,7,15,*]

[1]The Molecular Biology of Metabolism Laboratory, The Francis Crick Institute, London NW1 1AT, UK
[2]Department of Biochemistry, University of Cambridge, Cambridge CB2 1QW, UK
[3]Department of Biochemistry, Charité – Universitätsmedizin Berlin, 10117 Berlin, Germany
[4]Synthetic and Systems Biology Unit, Institute of Biochemistry, Biological Research Centre, Eötvös Loránd Research Network, Szeged 6726, Hungary
[5]HCEMM-BRC Metabolic Systems Biology Lab, Szeged 6726, Hungary
[6]Precision Proteomics Center, Swiss Institute of Allergy and Asthma Research (SIAF), University of Zurich, 7265 Davos, Switzerland
[7]The Wellcome Centre for Human Genetics, Nuffield Department of Medicine, University of Oxford, Oxford OX3 7BN, UK
[8]Core Facility – High Throughput Mass Spectrometry, Charité – Universitätsmedizin Berlin, 10117 Berlin, Germany
[9]Quantitative Gene Expression Research Group, MRC London Institute of Medical Sciences (LMS), London W12 0HS, UK
[10]Quantitative Gene Expression Research Group, Institute of Clinical Sciences (ICS), Faculty of Medicine, Imperial College London, London SW2 2AZ, UK
[11]Department of Biology and Biological Engineering, Chalmers University of Technology, 412 96 Gothenburg, Sweden
[12]Randall Centre for Cell & Molecular Biophysics, King's College London, New Hunt's House, Guy's Campus, London SE1 1UL, UK
[13]Institute of Biotechnology, Life Sciences Center, Vilnius University, Vilnius 10257, Lithuania
[14]Department of Biology, College of Science, United Arab Emirates University, P.O.Box 15551, Al-Ain, United Arab Emirates
[15]Lead contact
*Correspondence: claramelo85@gmail.com (C.C.-M.), markus.ralser@charite.de (M.R.)
https://doi.org/10.1016/j.cell.2022.12.007

SUMMARY

Metabolism is deeply intertwined with aging. Effects of metabolic interventions on aging have been explained with intracellular metabolism, growth control, and signaling. Studying chronological aging in yeast, we reveal a so far overlooked metabolic property that influences aging via the exchange of metabolites. We observed that metabolites exported by young cells are re-imported by chronologically aging cells, resulting in cross-generational metabolic interactions. Then, we used self-establishing metabolically cooperating communities (SeMeCo) as a tool to increase metabolite exchange and observed significant lifespan extensions. The longevity of the SeMeCo was attributable to metabolic reconfigurations in methionine consumer cells. These obtained a more glycolytic metabolism and increased the export of protective metabolites that in turn extended the lifespan of cells that supplied them with methionine. Our results establish metabolite exchange interactions as a determinant of cellular aging and show that metabolically cooperating cells can shape the metabolic environment to extend their lifespan.

INTRODUCTION

Metabolism determines the aging process at multiple levels, and this includes the formation of metabolites required for growth, cellular repair, and homeostasis.[1–3] At the same time, metabolism also generates reactive molecules, such as superoxide or methylglyoxal, and the equilibrium between protective and damaging molecules is a critical determinant of lifespan.[4–6] Moreover, key metabolic signaling systems, such as the AMP-activated protein kinase (AMPK) and the target of rapamycin (TOR) pathways, are equally central pathways regulating cellular aging and lifespan.[7–9]

An increasingly recognized property of metabolism is that it not only occurs inside cells, but it also involves the exchange of metabolites between cells and tissues and their environment.[10–13] Metabolite exchange interactions emerge because cells export metabolites for both biophysical and biochemical reasons, including membrane leakage, promiscuous metabolite transport, and the balancing of metabolic fluxes.[12,14–17] Moreover, cells possess an array of metabolite sensing and uptake systems.[8,18,19] In microbes, metabolite exchange interactions can be cooperative, competitive, or neutral,[13,20] but in any case, the exchange of metabolites

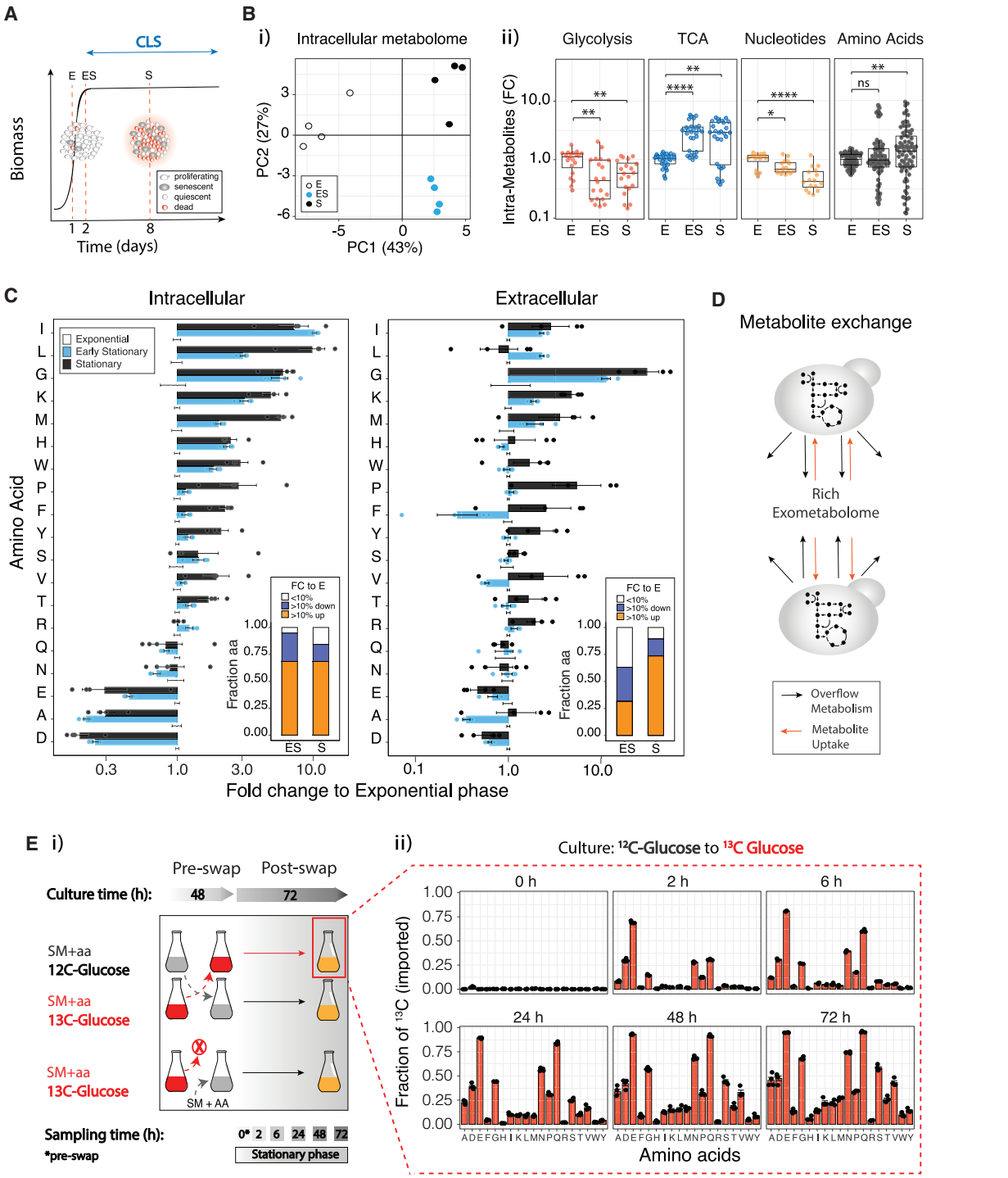

Figure 1. Yeast cells establish cross-generational metabolite exchange interactions

(A) Growth phases of yeast in batch culture, and the measurement of chronological lifespan (CLS) as survival in the stationary phase. E, exponential growth phase; ES, early stationary phase; and S, stationary phase; indicating 1, 2, and 8 days from culture start, respectively. Red dotted lines indicate the time points of sample collection for analysis.

(B) Targeted metabolome analysis for the quantification of intracellular nucleotide, amino acid, glycolytic, and tricarboxylic acid (TCA) cycle metabolites in wild-type yeast cells cultured in synthetic minimal (SM) medium at E, ES, and S phases, as described in (A). (i) Principal-component analysis (PCA); individual dots represent independent cultures. (ii) Intracellular metabolite concentrations shown as fold change (FC) to the exponential phase according to metabolite classes and growth phases. Boxplots represent median (50% quantile, middle line) and lower and upper quantiles (lower [25% quantile] and upper [75% quantile],

(legend continued on next page)

influences a broad range of physiological properties. Metabolic pathways are highly interconnected, so when a cell changes from the self-synthesis to the use of an available metabolite, a broad range of phenotypes can be altered. For example, cells taking up lysine from the environment mount better protection against oxidants, via increased pools of reduced nicotinamide adenine dinucleotide phosphate (NADPH) and reduced glutathione (GSH),[21] and cells that have a greater efflux activity because they cooperate metabolically, export drugs faster, and are more tolerant against antimicrobials.[22]

The role of cell-cell metabolic interactions in the aging process is barely understood.[2] Herein, we uncovered a role of metabolite exchange interactions in cellular aging by studying the metabolism of budding yeast during chronological lifespan (CLS). CLS, monitoring the survival of cells in stationary phase (postmitotic cells), is a basic aging model that was pivotal in understanding the critical role of conserved regulatory pathways such as the AMPK/sucrose non-fermenting 1 (SNF1, yeast homolog of AMPK) and TOR pathways in cellular aging.[23–27] We observed that metabolites exported by young, exponentially growing cells are re-imported during the stationary phase when cells age chronologically, indicating the existence of cross-generational metabolic interactions. Increasing metabolic interactions between cells through the use of self-establishing metabolically cooperating communities (SeMeCo),[22,28] increased longevity of the communities. In the search of the underlying mechanisms, we discovered a role for an altered extracellular metabolic environment that is rich in glycerol and that increases the lifespan of the different community members. In SeMeCo, we can explain the formation of this lifespan-extending exometabolome with the metabolic adaptations in methionine consumer cells. These obtain a more glycolytic metabolism and overflow glycerol, extending the lifespan of the methionine producers via a paracrine effect and by inducing lifespan-extending metabolic adaptations, including increased levels of antioxidant metabolites and polyamines.

RESULTS

Yeast cells establish cross-generational metabolite exchange interactions

To study metabolism during CLS experiments, we used a descendant of the commonly used yeast lab strain BY4741,[29] in which its biosynthetic deficiencies (auxotrophies) in three amino acids (*his3Δ1*, *leu2Δ*, and *met15Δ*) and one nucleobase (*ura3Δ*) were repaired through genomic integration of the wild-type alleles.[21] The cells were grown in a minimal nutrient media (synthetic minimal [SM] media[30] lacking amino acid supplements) in batch culture through exponential, early stationary, and stationary phases (Figure 1A). We then used a targeted metabolomics method[31] and quantified intracellular amino acids and nucleotides, as well as glycolysis and tricarboxylic acid (TCA) cycle intermediates. The metabolic profiles clustered in a principal-component analysis (PCA) according to growth phase (Figure 1Bi). The metabolite concentration changes reflected known metabolic transitions[32–34]: Consistent with a shift from fermentation to oxidative metabolism, the overall concentration of glycolytic metabolites decreased, whereas the concentration of TCA-derived metabolites increased. Moreover, the concentration of nucleotides decreased during early stationary and stationary phases, when growth ceases[34] (Figures 1Bii and S1A). Notably, however, while the median concentration of overall amino acids increased in the stationary phase, we observed a spread in the concentration range (Figure 1Bii). For example, isoleucine (I), glycine (G), and leucine (L) increased from exponential to stationary phase, but aspartate (D), alanine (A), and glutamate (E) decreased (Figure 1C). As amino acids are exported by yeast cells into the surrounding environment,[15,28,35–37] we quantified extracellular amino acid pools.[38] Despite having inoculated the cells in a minimal medium lacking amino acid supplements, we found that by mid-log phase (exponential phase) yeast cells had exported amino acids to reach significant extracellular concentrations and that 14 of the 19 analyzed amino acids were increased by >10% in early stationary or stationary phase (Figure 1C inset). Only alanine (A), aspartate (D), phenylalanine (F), and valine (V) were decreased during early stationary phase, and only aspartate (D) and glutamate (E) were reduced in stationary phase, compared to exponential phase (Figure 1C).

Sources of extracellular metabolites are their release from metabolically active cells, but also cell death. However, most of the metabolites already increased in the exponential and early stationary phases where cell death is negligible (~95% live cells) (Figure S1Bi), indicating that the main source of the increased metabolite concentrations is export from the metabolically active cells. Indeed, in stationary cultures, the concentration of metabolites did not correlate with the number of live cells (Figure S1Bii).

respectively) of pooled metabolite levels of n = 4 biological replicates. Each dot represents a metabolite in a biological replicate. Adjusted p values *p < 0.05, **p < 0.005, ***p < 0.0005, and ****p < 0.00005; adjusted p values in Table S1.

(C) Intracellular and extracellular amino acids levels in wild-type cultures during E, ES, and S phases, as described in (A). Bar plots show mean ± SEM FC to levels in E of n = 4 biological replicates. Adjusted p values in Table S1.

Insets represent the fraction of amino acids (from a total of 19) that show minimal, decreased, or increased changes in the FC to E, as shown by FC < 10%, FC > 10% down, and FC > 10% up, respectively.

(D) Metabolites are exported for different reasons, including to maintain metabolic homeostasis via overflow metabolism, contributing to the exometabolome. At the same time, cells sense and import metabolites from the surrounding environment. These dynamic export/import processes result in the exchange of metabolites between co-growing cells and the establishment of intercellular metabolic interactions.

(E) (i) Prototrophic wild-type yeast cells supplemented either with ^{12}C- or ^{13}C-glucose, followed by media swap for isotope tracing amino acid analysis, using targeted metabolomics[38] (see STAR Methods). (ii) Fractions of ^{13}C-labeled amino acids in cultures initially grown in ^{12}C-glucose and swapped to ^{13}C-glucose, at different time points post media swap, as described in (i). Bar plots show mean ± SEM of 4 biological replicates (individual dots represent independent cultures); individual fraction values and p values in Table S2.

Statistics for (B), (C), and (E) by unpaired two-sided Wilcoxon rank-sum test and multiple testing correction using the Benjamini-Hochberg (BH) method.

See also Figure S1.

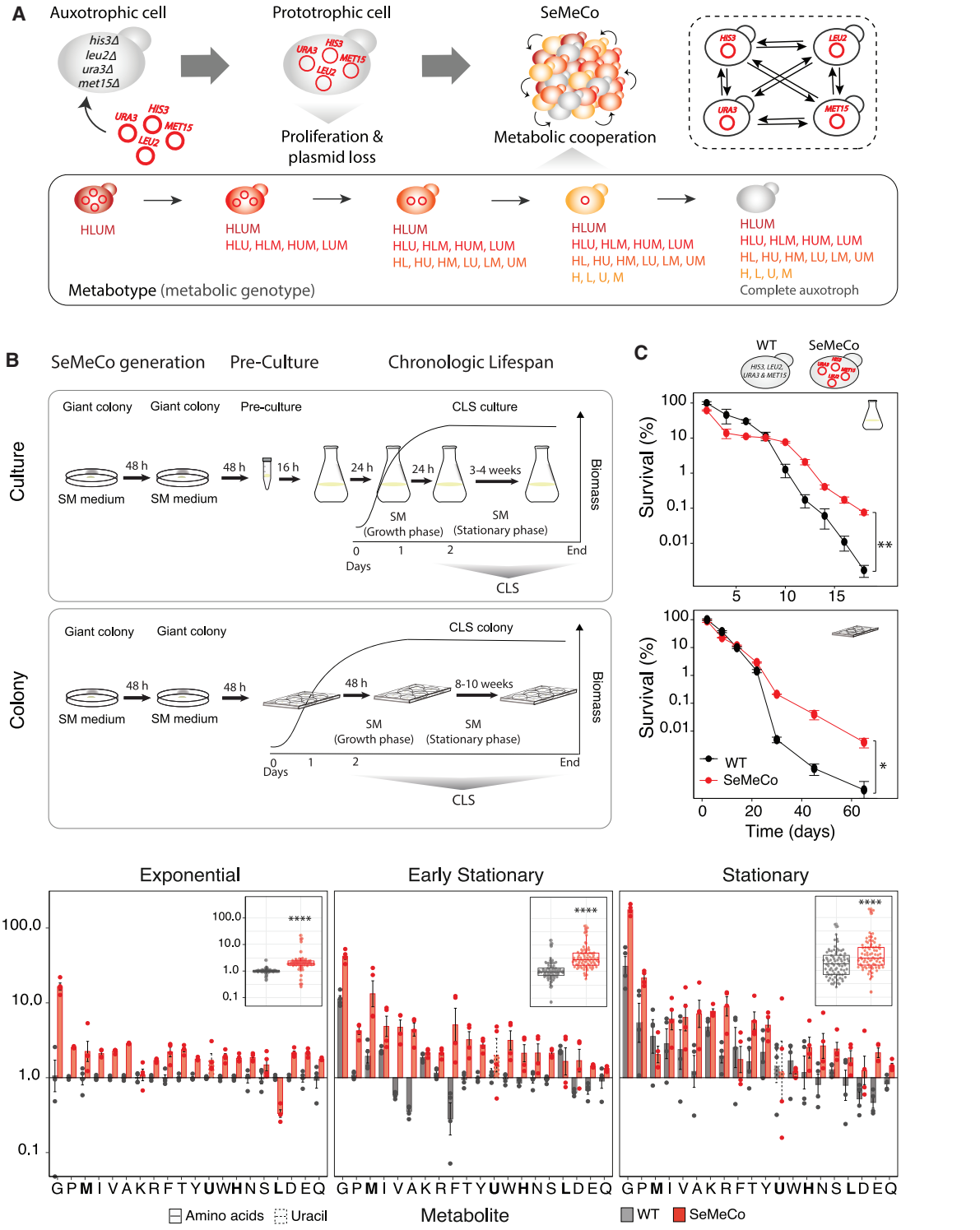

Figure 2. Metabolite exchange interactions extend lifespan in yeast communities

(A) SeMeCo start with a prototrophic cell that carries essential metabolic markers on single-copy plasmids (herein p*HIS3*, p*LEU2*, p*MET15*, and p*URA3*). When this cell grows into a community, the stochastic plasmid segregation leads to an increasing number of auxotrophs until an equilibrium of auxotrophs (metabolite consumers) and complementary prototrophs (metabolite producers) is reached.[28,39]

(B) CLS of wild-type communities and SeMeCo start by spotting giant colonies twice to ensure cell proliferation, plasmid segregation, and ultimately cross-feeding between auxotrophs and prototrophs (SeMeCo generation), followed by (top) pre-culture and culture for "culture" or (bottom) giant colony spotting for "colony" CLS, respectively.

(legend continued on next page)

Because microbial cells efficiently sense and take up extracellular amino acids,[18,35] we speculated that cells during the stationary phase could take up these amino acids (Figure 1D). We exploited ^{13}C-glucose isotope labeling to test for the consumption, by stationary cells, of metabolites that had been produced during the exponential phase. We cultured wild-type yeast cells on SM media supplemented with ^{12}C- or ^{13}C-glucose for 48 h, a duration which ensured that the glucose in the media had been exhausted—catabolized into unlabeled (^{12}C) or labeled (^{13}C) metabolites, respectively. We then swapped the media between labeled and unlabeled cells. In parallel, we set control cultures growing on SM media supplemented with ^{13}C-glucose, which were then swapped into SM media supplemented only with amino acids (without glucose), to distinguish whether intracellular amino acid levels were a direct result of import or indirectly derived from catabolism of imported carbohydrates (Figure 1Ei). Levels of fully labeled (^{13}C) or unlabeled (^{12}C) intracellular amino acids (from glucose catabolism) were quantified using a targeted metabolomics method.[38] Growth on SM media supplemented with ^{12}C- or ^{13}C-glucose did not change cell growth parameters prior or post swap (Figures S1C and S1D). These experiments confirmed that the amino acids released by cells in the exponential phase are taken up by the stationary cells, as shown by the increased intracellular levels of ^{13}C- or ^{12}C-containing amino acids in cultures initially grown on ^{12}C- or ^{13}C-glucose, respectively (Figure 1Eii and S1E). Hence, yeast cells establish cross-generational metabolite exchange interactions during chronological aging.

Metabolite exchange interactions extend lifespan in yeast communities

We next questioned what impact the exchange of metabolites might have on CLS. Because metabolite export from cells is a basic property of metabolism that cannot be prevented, we used an approach in which metabolite exchange interactions were increased to test the influence of metabolite exchange on CLS. Metabolite exchange interactions are increased in SeMeCo in which the segregation of plasmids that encode essential metabolic enzymes stochastically introduces auxotrophies (metabolic deficiencies) during colony formation.[28,39] SeMeCo form a community containing auxotrophs that grow as a community on the basis of obligate metabolite sharing (Figure 2A). Cells in SeMeCo do not have altered biosynthetic pathways and are not rendered feedback resistant, as compared with engineered metabolite sharing communities.[40] Instead, they boost the number of metabolic interactions occurring between cells because plasmid segregation continues until an equilibrium is reached between metabolite-consuming and -producing cells.[28] Compared to wild-type communities, SeMeCo are characterized by overall increased metabolite export activity with increased extracellular metabolite concentrations.[22]

Analyzing the CLS of SeMeCo (Figure 2B) by monitoring colony-forming units (CFUs) over time, we observed that in comparison with the wild-type strain, SeMeCo were long-lived. SeMeCo lost more CFUs immediately after reaching the stationary phase, but in later time points contained more CFUs and were alive after the wild-type cultures lost viability (Figure 2C). To have an independent assessment of survival, we also monitored cell viability using live/dead cell staining assays. At late time points, SeMeCo also contained significantly more viable cells (Figure S2A).

The lifespan extension in SeMeCo is mediated by a paracrine mechanism

We observed that yeast cells survived much longer in colonies than in liquid culture (~65 vs. 20 days), with SeMeCo still presenting a significantly longer CLS than wild-type cells (Figure 2C). This result was consistent with the notion that metabolic interactions could serve as an explanation for the increased CLS; the close proximity of cells in colonies reduces the dilution of extracellular metabolites, which is beneficial for metabolic interactions.[41] Indeed, we found higher extracellular levels of amino acids and uracil in aging SeMeCo when comparing with wild-type cultures (Figure 2D).

We continued testing whether the differences in lifespan between SeMeCo and wild type could be explained by differences in culture pH,[42] which can change depending on its metabolite composition, but we detected no significant differences (Figure S2B). Next, we tested if the lifespan extension is associated with specific metabolic pathways. The SeMeCo model is based on the stochastic segregation of four plasmid-encoded auxotrophic marker enzymes (*HIS3, LEU2, URA3*, and *MET15*), resulting in 16 metabotypes (metabolic genotypes, Figure 2A), which are characterized by a broad range of metabolic and transcriptional differences.[43] We monitored absolute occurrence and relative contributions of the different metabotypes. The absolute CFU numbers decreased for all metabotypes (Figure S2C), accompanying the overall loss of cell viability without further proliferation in the stationary phase. However, the relative proportion of prototrophic cells declined over time. During the late stationary phase, ~98% of viable cells were auxotrophs for at least one metabolite. Among the auxotrophs, the *MET15* segregants dominated (Figures 3A and S2C).

We therefore generated additional SeMeCo in which only three markers segregate (“3p-SeMeCo”), and the fourth locus

(C) (Top) Culture and (bottom) colony CLS of wild type and SeMeCo, by CFU analysis (see STAR Methods). Data are mean ± SEM survival (percentage FC), compared with wild-type mean survival at the beginning of the stationary phase; n = 4 biological replicates/strain (culture CLS) or n = 3 biological replicates/strain (colony CLS). p values in Table S3.

(D) Extracellular amino acids and uracil levels, measured by targeted metabolomics[38] (see STAR Methods), in wild-type and SeMeCo cultures during CLS. Bar plots show mean ± SEM FC to mean wild-type levels in the exponential phase of n = 4 biological replicates/strain. The shared essential metabolites in SeMeCo—H, L, U, and M—are highlighted in bold. Insets boxplots represent median (50% quantile, middle line) and lower and upper quantiles (lower [25% quantile] and upper [75% quantile]) of pooled metabolite levels of 4 biological replicates/strain/growth phase; each dot represents a metabolite in a biological replicate. Adjusted p values in Table S1.

Statistics by unpaired two-sided t test (C) and Wilcoxon rank-sum test (D) and multiple testing correction using the BH method. p value *p < 0.05, **p < 0.005, ***p < 0.0005, and ****p < 0.00005.

See also Figure S2.

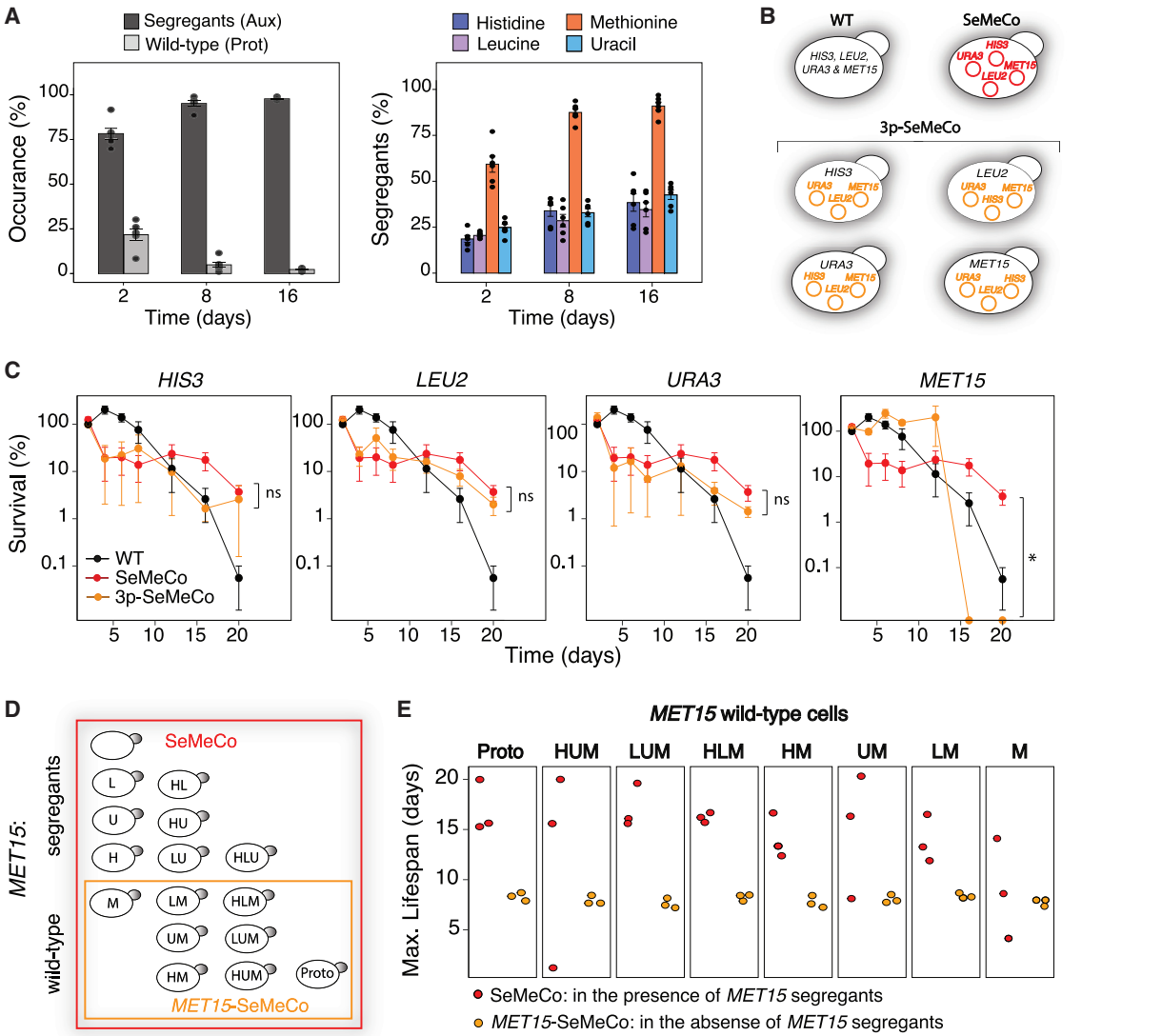

Figure 3. The lifespan extension in SeMeCo is mediated by a paracrine mechanism

(A) (Left) Frequency of overall segregant (at least one auxotrophy) and prototrophic (bearing the four wild-type loci) cells during CLS. (Right) Frequency of the individual segregants, i.e., per auxotrophy for H, L, U, or M over time (see STAR Methods). Bar plots show the mean ± SEM of n = 6 independent SeMeCo cultures across 2 independent experiments (dots represent independent cultures). p values in Table S4.

(B) Wild type, SeMeCo, and four 3p-SeMeCo, in which one of the markers (*HIS3*, *LEU2*, *MET15*, or *URA3*) is genomically integrated and no longer segregates (see STAR Methods).

(C) CLS of wild type, SeMeCo, and 3p-SeMeCo, by high-throughput CFU (HTP-CFU) (see STAR Methods). Data are mean ± SEM survival (percentage FC) compared with wild-type mean survival at the beginning of the stationary phase; n = 4 biological replicates/strain. Survival curves are shown separately for visualization purposes (all strains were cultured and analyzed in parallel). p values in Table S3.

(D) The segregation of the four metabolic markers gives rise to 16 different metabotypes, eight of which have segregated the *MET15* plasmid (Figure 2A).

(E) Maximum lifespan of the eight *MET15* wild-type (prototrophic) metabotypes, in the presence (SeMeCo, red) or absence (*MET15*-SeMeCo, yellow) of *MET15* segregants (see STAR Methods). Dots are independent cultures per SeMeCo type. Data are from n = 3 biological replicates/SeMeCo. p values in Table S4.

Statistics by paired two-sided t test (A); unpaired two-sided (C) and one-sided (E) Wilcoxon rank-sum test; p value *p < 0.05 and ns p > 0.05.

See also Figures S2–S4.

is genomically repaired (Figure 3B). The genomic repair of *HIS3, LEU2*, or *URA3* did not significantly change the lifespan. However, the 3p-SeMeCo, in which the *MET15* locus was no longer segregating, had a significantly shorter lifespan (Figure 3C). Conversely, a SeMeCo that only segregated the *MET15* marker (p*MET15*-SeMeCo, also termed pM-SeMeCo) had an increased lifespan, compared with wild-type communities (Figure S2D).

Methionine biosynthesis and associated sulfur-containing intermediates have repeatedly been linked to aging, as lifespan extensions were observed upon methionine restriction in model

organisms.[44–50] Interestingly, however, as shown above, the extracellular medium was generally more amino acid rich in SeMeCo than in wild-type cells (Figure 2D), indicating that within the SeMeCo, lifespan extension is not mediated by methionine restriction. Furthermore, we supplemented wild-type and *met15Δ* cells with 20 mg/L of methionine, a standard culture concentration. Despite the high methionine levels, we observed a robust lifespan extension in *met15Δ* cells and in SeMeCo that segregate the *MET15* plasmid (Figure S2D). Our data also suggest that the lifespan difference is not mediated by a difference in growth rate.[51] We observed that SeMeCo growth rate in SM cultures is decreased, compared with wild-type communities (Figure S2E); however, the growth rate in both the SeMeCo and *MET15*-SeMeCo is similar, and hence not causal to their diverging lifespans.

Eventually, we found evidence for a paracrine effect that underlies the lifespan extension. We coupled a CLS experiment (Figure S2F) to metabotyping analysis (see STAR Methods). We noted that not only was the lifespan of *met15Δ* cells increased, but the presence of the *met15Δ* cells also increased the maximum lifespan of the other cells in the community (Figures 3A, 3D, and 3E). An exception were the cells that had segregated all but the *MET15* plasmid; these had a similar lifespan (in average) to the control cells in which *MET15* was genomically repaired (Figure 3E, panel M). This result pointed us to changes in the exometabolome as a source of the lifespan extension.

Methionine auxotrophy and methionine exchange is frequent in nature

SeMeCo are a laboratory model to study metabolic interactions. We therefore questioned how frequent interactions between methionine auxotrophs and prototrophs could be in nature. Using the auxotrophy predictions[52] from the metagenomic data of the >12,000 natural prokaryotic communities collected in the Earth Microbiome Project,[53] we found that methionine auxotroph frequency is in the mid-range among all amino acid auxotrophies (bacterial and archaea samples). Of these natural microbial communities, 67.9% contained at least one species predicted to be auxotrophic for methionine, with some communities containing >40 species auxotrophic for methionine (Figure S3A).

Nonetheless, analyzing only the number of auxotrophs will underestimate the number of potential methionine consumers, as not only auxotrophs but also methionine prototrophs take up amino acids once they become available. Therefore, to determine which extracellular levels of methionine are necessary for cells to switch from being a methionine producer to being a methionine consumer, we used ^{13}C isotope labeling and generated a "switching curve" in the prototrophic yeast strain. We found that yeast cells switch at nanomolar extracellular concentrations (Figure S3B). Thus, low extracellular methionine concentrations are sufficient to convert a prototrophic yeast cell from a methionine producer to a cell that takes up the metabolite. We also conducted a complementary proteomics experiment, where we recorded proteomes for the same prototrophic yeast strain with and without a mixture of amino acid supplementation. We founnd that prototrophic cells are highly responsive to the presence of amino acids. Strikingly, the methionine biosynthetic enzymes were the most responsive, showing on average a 4- to 8-fold downregulation (Figure S3C). These results provide complementary evidence that the prototrophs respond to the presence of extracellular amino acids and, together with the uptake of methionine, downregulate the biosynthetic pathway.

Furthermore, using proteome data[54] recorded for a collection of >1,000 wild yeast strain isolates,[55] we found remarkable diversity in the expression level of genes associated with the methionine pathway, showing that the expression of the methionine biosynthetic pathway is generally heterogeneous in natural yeast communities (Figure S3D).

Finally, heterogeneity in the expression of *MET15* has been reported in aging isogenic yeast colonies, coupling protein fluorescence tagging and colony cross-section microscopy.[56] Čáp et al. also found that metabolic biosynthesis and transport mutants impact the development and survival of subpopulations of cells in a colony.[56] Taken together, the results suggest that heterogeneity in the methionine pathway affects aging under different conditions.

Lifespan extension in cooperating communities is mediated by protective overflow metabolites

To explore the cell-extrinsic factors that mediate the lifespan extension phenotype, we started by simulating the likely metabolite changes in the SeMeCo using a community-adapted version of the metabolic flux balance analysis (FBA).[22] We simulated the exchange of metabolites between a prototroph and each of the 15 auxotrophic metabotypes that emerges from all possible combinations of H, L, U, and M auxotrophies (Figure S4A). The community FBA revealed that interactions between *MET15* and *met15Δ* cells cause broad metabolic flux changes, notably, including central metabolism, and the exchange of a larger number of metabolites beyond methionine (Figure S4B). We investigated the generality of our findings by expanding our analysis to other amino acid exchange interactions, using a genome-scale FBA of auxotroph-prototroph communities. We found that there is a tight interaction between the metabolic pathways and that, interestingly, a large number of metabolic transitions act on the flux of the methionine pathway (Figure S4C), suggesting our results might be of relevance to a broader range of metabolite exchange interactions that often converge on this pathway.

In order to obtain a deeper understanding of the pathways involved, we continued with proteome analysis. Performing untargeted proteomics[57,58] on chronologically aging wild-type communities and SeMeCo that segregate or do not segregate the *MET15* marker (Figure 4A), we quantified 1,951 proteins, around half the typically expressed yeast proteome.[59] The first principal component (PCA1) in a PCA explained 33% of the variance and separated the proteomes according to growth phase. The second principal component (PCA2), explaining 23% of the variance and separated the samples based on whether the communities segregated the *MET15* marker (Figures 4B and S5A). Moreover, a comparison of the different communities revealed that most of the differential protein expression occurs when *MET15* and *met15Δ* cells interact (Figures 4C and S5B). Gene ontology (GO) enrichment analysis revealed that >50% of the differentially expressed proteins comprised GO slim terms

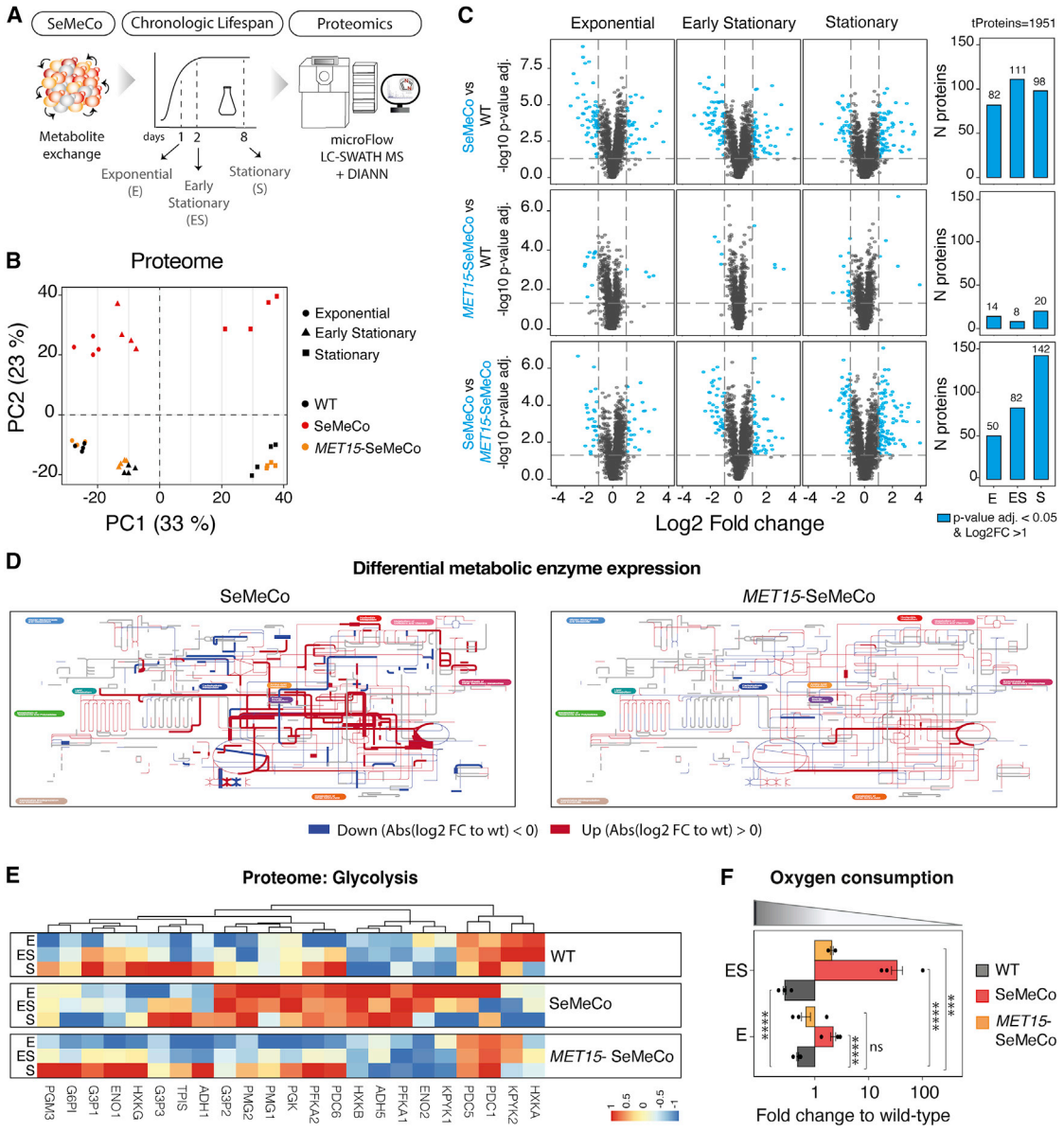

Figure 4. Proteomic and metabolomic changes in yeast communities where *MET15* and *met15Δ* cells interact reveal an increased glycolytic metabolism

(A) Untargeted proteomics analysis[57,58] of chronologically aging (Figure 1A) wild type, SeMeCo, and *MET15*-SeMeCo (see STAR Methods), performed on four biological replicates/strain.

(B) PCA of the proteomes described in (A). Individual data points represent biological replicates/strain.

(C) (Left) Volcano plots showing differential protein expression as $\log_2$ fold change (FC) between strains and $-\log_{10}$ adjusted p value. Blue dots denote proteins above an absolute (Abs) $\log_2$ FC of 1 (vertical dashed lines) and adjusted p value < 0.05 (horizontal dashed line). (Right) Number of proteins defined as per blue dots (in the volcano plots), from the total proteins quantified (tProteins), represented as bar graphs, per growth phase and pairwise comparison between strains. Adjusted p values in Table S5.

(D) Differential metabolic enzyme expression levels mapped to a yeast metabolic network graph using iPath3,[60] shown in the ES phase; E and S phases are shown in Figure S5D. Red and blue lines represent significantly upregulated or downregulated proteins in SeMeCo and *MET15*-SeMeCo when compared with wild type; gray lines represent non-mapped/absent proteins in the measured proteomes. Thickness of the lines represents Abs($\log_2$FC) changes (thickening = increased Abs($\log_2$FC)).

(E) Expression of enzymes belonging to the glycolytic pathway (UniProt protein name, columns), derived from the proteome analysis in (A) and normalized to a −1 to 1 scale, per growth phase and yeast communities (rows).

(F) Oxygen (O_2) consumption, as measured by O_2 saturation in culture in wild type, SeMeCo, and *MET15*-SeMeCo, in E and ES phases (see STAR Methods). Higher O_2 saturation in culture corresponds to lower oxygen comsuption. Data are mean ± SEM FC to wild-type mean levels; n = 3 biological replicates/strain. Individual dots represent independent cultures. p values in Table S6.

Statistics by unpaired two-sided t test and multiple testing correction using the BH method (C) and unpaired two-sided Wilcoxon rank-sum test (F).

See also Figure S5.

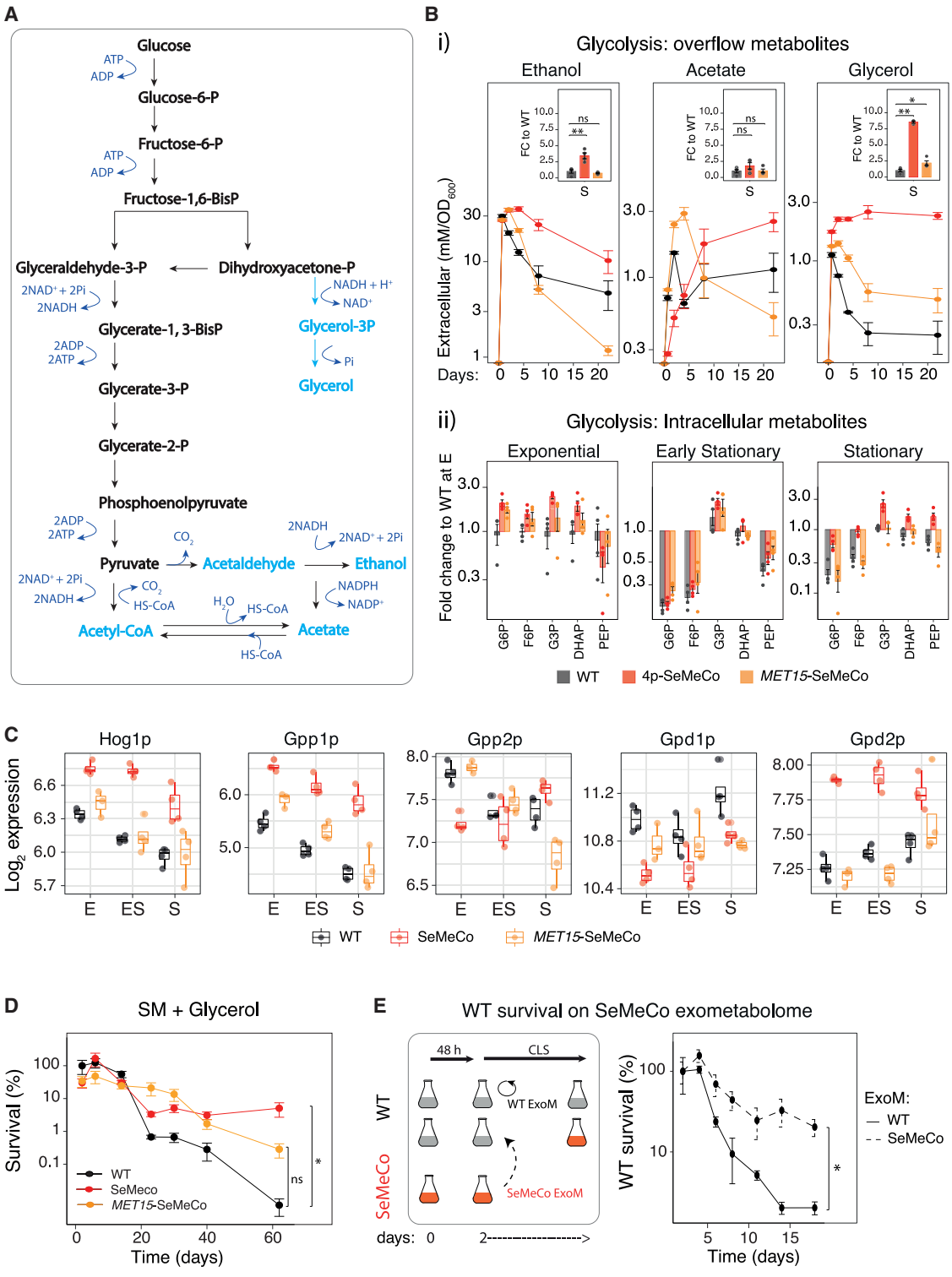

Figure 5. Lifespan extension in SeMeCo is promoted by a self-generated protective exometabolome

(A) Reaction scheme of glycolysis (Embden Meyerhoff Parnass pathway[104]), and associated metabolites generated during fermentation (light blue).

(B) Quantification of (i) ethanol, acetate and glycerol in the exometabolome, by HPLC, and (ii) intracellular glycolytic intermediates (G6P, glucose-6-phosphate; F6P, fructose-6-phosphate; PEP, phosphoenolpyruvic acid; DHAP, dihydroxyacetone phosphate; G3P, glyceraldehyde-3-phosphate), by targeted metabolomics[31] (see STAR Methods) of wild type, SeMeCo, and *MET15*-SeMeCo. Data are mean ± SEM metabolite levels; n = 4 biological replicates/strain. Insets in (i) indicate FC to mean wild-type levels in S phase (day 8); individual dots represent independent cultures. p values in Table S1.

(legend continued on next page)

belonging to metabolic processes (Figure S5C). Visualizing the enzyme expression levels by mapping them to a metabolic network graph using iPath3,[60] highlighted changes in central and intermediate metabolism (Figures 4D and S5D). A pathway-centric analysis of the proteome pointed our attention to glycolysis. Several glycolytic enzymes were upregulated in the communities that contained *MET15* segregants (Figure 4E). However, because stationary cells typically rely on oxidative phosphorylation for energy production,[32] the increase of glycolytic enzyme expression was somewhat surprising. We therefore conducted oxygen consumption (OC) analysis in exponential and early stationary phase cultures, excluding stationary phase to avoid confounding effects produced by an increasing proportion of dead cells. Consistent with the upregulation of glycolysis at the proteome level, we found that the OC was reduced in the communities containing the *MET15* segregants (Figure 4F).

Both glycolytic activity and glycolytic overflow metabolites (Figure 5A) are associated with chronological aging. Glucose restriction itself extends lifespan,[61] and the glycolytic overflow metabolites ethanol and acetate shorten lifespan,[42,62] while a third overflow metabolite, glycerol, increases CLS.[63] We measured ethanol, acetate, and glycerol in the exometabolome of the different SeMeCo and wild-type communities. In the stationary phase, levels of all three metabolites were higher in the communities where *MET15* and *met15Δ* segregants interacted. While ethanol and acetate levels were ~2-fold increased, stronger changes were observed for glycerol, whose levels were ~8-fold increased during stationary phase (Figure 5Bi).

In order to explain the sources of the increase in glycerol, we studied the intracellular glycolytic metabolome. SeMeCo revealed concentration changes in upper and lower glycolytic metabolites across all growth phases: the most notable changes were detected in the glycerol-associated three-carbon phosphates (G3P and dihydroxyacetone phosphate [DHAP]) in the stationary phase. These were increased specifically in the communities where *MET15* and *met15Δ* cells interacted (Figure 5Bii)). Further, we analyzed the expression of enzymes specifically regulating glycerol biosynthesis. We found that expression of the high-osmolarity glycerol 1 protein (Hog1p), a kinase from the high-osmolarity glycerol (HOG) pathway with transcriptional regulatory activity over genes involved in response to osmotic stress, including glycerol biosynthetic enzymes, is significantly upregulated in SeMeCo vs. wild-type communities. Moreover, expression of the glycerol biosynthetic enzymes glycerol-3-phosphate phosphatase 1 and 2 (Gpp1p and Gpd2p) was also increased (Figure 5C).

To test whether the accumulation of glycerol could be associated with the extended lifespan, we performed a CLS assay where cells were grown in SM media supplemented with glycerol. Glycerol supplementation extended lifespan to 62 days of culture, as compared with the previously observed (Figure 3C) ~20 days in wild-type and *MET15*-SeMeCo. The SeMeCo also profited from the glycerol treatment, although the absolute values were shifted due to their overall longer lifespan (Figure 5D).

While these results demonstrated that glycerol accumulation is beneficial, the glycerol increase alone might not sufficiently reflect the complexity of the yeast exometabolome. To validate if the community's self-generated exometabolome is indeed mediating the lifespan extension, we complemented these results with a media swap experiment. We cultured wild-type communities in SM media until the early stationary phase and then transferred them to a SeMeCo exometabolome (generated in parallel). Control cultures were generated by placing wild-type communities back in their own exometabolome (Figure 5E). Wild-type communities cultured on the exometabolome harvested from SeMeCo showed significant lifespan extension, representing a 10-fold increase in CFU formation at 18 days of culture (Figure 5E). Hence, the metabolic changes emerging when *MET15* and *met15Δ* cells interact generate a pro-survival metabolic environment that extends lifespan of all cells in a community.

Methionine exchange interactions impacts multiple aging pathways

Metabolism and aging are deeply interlinked, with multiple pathways coordinating metabolism also being major regulators of aging and lifespan (Figure 6A). Sulfur amino acids and associated intermediates, as part of the methionine biosynthetic pathway, are also key players in such pathways, directly impacting antioxidant response via biosynthesis of glutathione (GSH) and polyamines, with the latter also regulating multiple cellular processes[64] (Figure 6A). We therefore analyzed levels of these aging-regulating metabolites and associated biosynthetic enzymes. We detected increased expression of glutathione synthetase enzymes, such as the glutamylcysteine synthetase, glutathione synthetase and reductase (Gsh1p, Gsh2p and Glr1p; UniProt protein name: GSH1, GSHB and GLR1, respectively), with increased levels of GSH, while not detecting significant changes in reactive oxygen species (ROS), between SeMeCo and wild-type communities (Figure 6B).

Another critical group of anti-aging metabolites are polyamines, which include putrescine, spermidine, and spermine.[65] Polyamine biosynthesis requires *S*-adenosylmethionine (SAM), an intermediate of the methionine biosynthetic pathway, which is also a substrate for the generation of spermidine and spermine (Figure 6A). Increased levels of spermine and putrescine, but not spermidine, were detected in SeMeCo when compared with wild type or *MET15*-SeMeCo in the stationary phase (Figure 6C).

(C) Boxplots showing $\log_2$ expression levels of Hog1p and the glycerol biosynthetic enzymes Gpp1p/2p and Gpd1p/2p. Dots represent values for individual biological replicates; n = 4 biological replicates/strain. Data derived from proteome analysis in Figure 4A. Adjusted p value in Table S5.
(D) CLS, by HTP-CFU, of wild type, SeMeCo, and *MET15*-SeMeCo, cultured on SM supplemented with glycerol. Data are mean ± SEM survival (percentage FC) compared with mean wild-type survival at the beginning of the stationary phase; n = 4 biological replicates/strain. p values in Table S3.
(E) CLS, by HTP-CFU, of wild-type cultures swapped to SeMeCo culture media (SeMeCo exometabolome [exoM]) or kept in their culture media (WT exoM) at the start of stationary phase (see STAR Methods). Data are mean ± SEM survival (percentage FC) compared with mean wild-type survival at the beginning of stationary phase; n = 4 biological replicates/exoM. p values in Table S3.
Statistics by unpaired two-sided t test (B and C) and unpaired two-sided Wilcoxon rank-sum test (D and E); p values *$p < 0.05$, **$p < 0.005$, and ns $p > 0.05$. The different time scales (x axis) on (D) and (E) are due to survival differences in cultures under glycerol supplementation, as compared with growth on glucose.

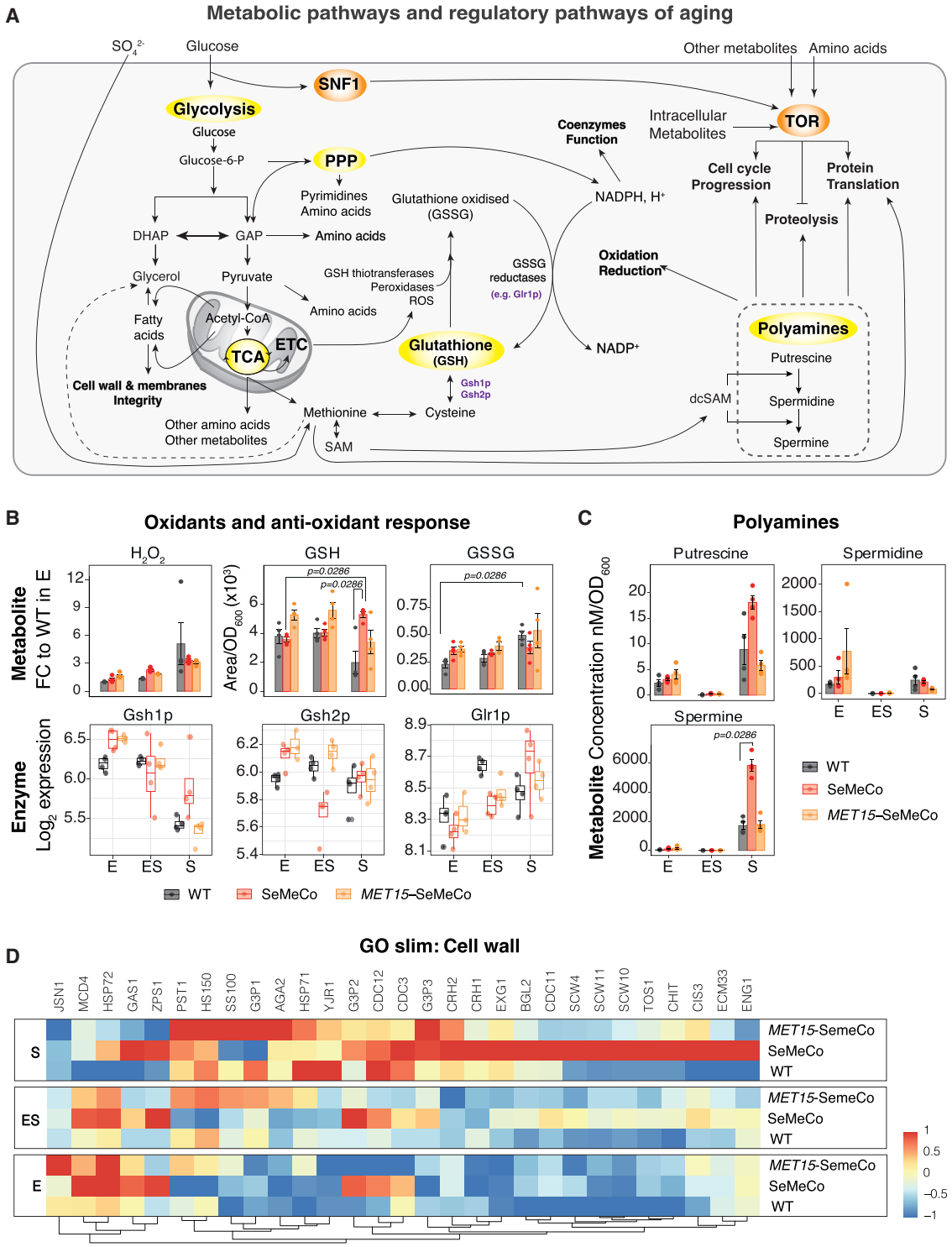

Figure 6. Methionine exchange interactions impact multiple biochemical processes of aging

(A) Metabolic pathways and regulatory pathways of aging with focus on the role of methionine in these processes.

(B) (Top left) H_2O_2 fold change (FC) levels to wild type in exponential phase, as measured by dihydrorhodamine 123 (DHR) intensity by flow cytometry and (top middle, right) levels of reduced and oxidized glutathione, GSH, and GSSG, respectively, as measured by targeted metabolomics[31] of wild-type communities and SeMeCo during E, ES, and S phases. Bar plots show the mean ± SEM of n = 4 biological replicates/strain. p values in Table S1. (Bottom) Boxplots represent median (50% quantile, middle line) and lower and upper quantiles (lower [25% quantile] and upper [75% quantile]) of $\log_2$ expression levels of glutathione

(legend continued on next page)

Next, we mined the proteome data for changes in targets of the SNF1 (AMPK) and TOR pathways. Overall, we did not find evidence of an increased starvation response in SeMeCo compared with wild type. Snf1p and related proteins, such as the SNF1-interacting protein 1 and 5 (Sip2p and Sip5p) and resistance to glucose repression protein 1 (Reg1p), increased in early stationary and stationary phases, compared with exponentially growing cells, but no significant differences were observed between wild-type and SeMeCo, except for Reg1p, a protein involved in negative regulation of glucose-repressible genes (Figure S6A). Gene sets associated with TOR activity were not specifically enriched in SeMeCo versus wild-type during CLS (Figure S6B). Instead, our data show that expression of enzymes participating in metabolic processes in general, and amino acid biosynthesis in particular, is upregulated at the proteome level (Figures 4D, S5C, and S5D) and that amino acid levels are increased in SeMeCo, as compared with wild-type communities, throughout CLS (Figure 2D). This corroborates our previous observations, using genome-scale metabolic modeling, metabolome, and proteome analysis, whereby auxotrophs upregulate a broad range of metabolic pathways when interacting with prototrophs.[22] Supporting a role for the exometabolome pro-survival metabolite glycerol, proteins involved in osmoregulation and glycerol-dependent lipid biosynthesis were significantly upregulated in SeMeCo, as compared with wild type (Figure S6C). Glycerophospholipids are critical for maintaining cell wall integrity, a process that is compromised during aging.[66] Indeed, we found that proteins belonging to the GO slim term "cell wall" were also upregulated in SeMeCo vs. wild-type communities (Figure 6D). In summary, our data show that multiple metabolic anti-aging factors, such as expression of antioxidant enzymes, antioxidant metabolites, polyamines, and glycerol-associated pro-survival processes are increased when cells grow in the protective communal exometabolome.

DISCUSSION

The classical view of metabolism as a biochemical network operating inside the cell is increasingly replaced with one seeing metabolic networks spanning across cells and their environment. In microbes, metabolic networks can span not only over single but also over multiple species that interact within microbial communities.[37,67–69] When cells share metabolites or take them up from external sources, their physiology can be altered substantially. For instance, we previously showed that cells that take up lysine mount better protection against oxidants,[21] or that the presence of auxotrophs enriches metabolic environments and increases drug tolerance.[22] Studying the physiological impact of metabolite exchange interactions remains, however, technically challenging. Metabolite exchange interactions between cells are not captured by typical single-cell techniques, nor does the concentration of a metabolite explain whether it was produced or consumed by the analyzed cell. Moreover, it is difficult to address the problem with classic tools of genetics (e.g., knockouts or knockdowns) or inhibitors, because metabolite levels are driven by the activity of many transporters with a broad substrate spectrum; also, the inhibition of export and import of metabolites can cause broad changes in the interconnected metabolic network. We here address this problem by using a combination of various omics, metabolic modeling, and genetic approaches and by studying wild-type cells and metagenomic data, but also by making use of SeMeCos to boost metabolic interactions between communal cells.

In studying metabolite exchange interactions in the context of CLS in yeast, we made two major observations. The first is that metabolites exported during the exponential phase are imported by cells during the stationary phase, establishing a "cross-generational" exchange of metabolites, and that boosting such interactions increases lifespan. It is important to emphasise in this context that while exponential cells are temporally separated from the chronologically aging cells in a batch culture CLS experiment, both cell types co-occur within aging colonies,[41] and it is conceivable that the close physical proximity prevents dilution and simplifies the exchange of metabolites between cells.[70] Testing their lifespan, we noted that colonial cells lived much longer than the ones in culture, even in wild-type colonies.[41] The reasons are not fully understood, but it is consistent with our findings that an increase in metabolic interactions is beneficial for the lifespan of cells.

The second observation is that the lifespan extension is explained by the metabolic environment that the cells self-generate. Analysis of the metabotype composition within SeMeCo attributed a special role to the methionine biosynthetic pathway that is part of the organic sulfur cycle. We found that all metabotypes in the community live longer if the community contained *MET15* segregants. Indeed, sulfur amino acids,[71] including methionine, are known to play specific roles in the aging process. Methionine restriction in particular can extend lifespan in a number of organisms,[44–49] prevent the development of a variety of diseases,[72] and influence the response to anticancer therapies.[73,74] However, our results differed from many of these studies in a fundamental aspect, as they did not indicate that the lifespan extension was caused by methionine restriction. Instead, we found metabolic rearrangements to follow when cells switch from the biosynthesis to the uptake of methionine, including the release of glycerol in the extracellular space. The result is a protective metabolic environment in which not only

biosynthetic enzymes; n = 4 biological replicates/strain (dots represent values for independent culture). Data from the proteome analysis in Figure 4A. Adjusted p value in Table S5.

(C) Intracellular polyamines concentration, as measured by targeted metabolomics, of wild-type communties and SeMeCo during E, ES, and S phases. Bar plots show the mean ± SEM of n = 4 biological replicates/strain (dots represent independent cultures). p values in Table S1.

(D) Expression of proteins belonging to the GO slim term: "cell wall" (UniProt protein name, columns), derived from the proteome analysis in Figure 4A, per growth phase and yeast communities (rows). Data are the mean expression, normalized to a −1 to 1 scale, of n = 4 biological replicates/strain. Adjusted p value in Table S5. Statistics by unpaired Wilcoxon rank-sum test (B, top and C) and unpaired two-sided t test and multiple testing correction using the BH method (B, bottom and D). E, exponential; ES, early exponential; S, stationary phases. See also Figure S6.

the lifespan of methionine consumers but also the lifespan of methionine producer cells is increased.

When interrogating the generality of our findings, by expanding our analysis to other amino acid exchange interactions, we found a large number of metabolic transitions acting on the flux of the methionine pathway. We concluded that because a large number of different metabolic interactions will act on the flux of the studied biosynthetic pathway, and because of the protective effects mediated by the resulting exometabolome, our results are important not only specifically for the methionine segregants used as a model to study the process in SeMeCo, but they are also of relevance to understand a broader range of metabolite exchange interactions that often converge on this pathway.

In our mechanistic dissection of the cellular processes driving longevity in SeMeCo, we found that multiple protective mechanisms impacting aging and lifespan are increased when cells grow in the pro-survival exometabolome generated by the metabolite sharing cells, reinforcing the tight link between metabolic and aging-regulating processes. In a nutshell, SeMeCo presented a general increase in metabolic fluxes, metabolic enzyme expression, and increased metabolite levels. This included elevated polyamines and GSH levels with increased expression of antioxidant enzymes. Importantly, we found glycerophospholipid biosynthetic enzymes and cell wall assembly proteins to be upregulated in SeMeCo, compared with wild-type communities, processes that are positively linked to increased glycerol levels and to aging.[63,66,75–77]

Our results may also offer an explanation for other contexts whereby the organic sulfur cycle and linked pathways are altered independently of methionine restriction. For example, linking endocrine regulation and metabolic regulation, long-lived dwarf mice have altered methionine metabolism and improved oxidative defence, mostly via increased glutathione metabolism.[78] These mice have upregulated sulfur, methionine, and one-carbon metabolism pathways in a methionine restriction-independent way. Furthermore, endogenous hydrogen sulfide (H_2S) production, as part of the organic sulfur cycle,[79] is essential for the beneficial effects of dietary restriction[80] and has been shown to provide health benefits in experimental organisms, ranging from protection from ischemia/reperfusion injury to lifespan extension.[81] In yeast, H_2S extends CLS in a temporally resolved manner,[82] and a recent study in our lab found that *MET15* auxotrophs generate increased levels of H_2S,[83] hence it is possible that increased levels of H_2S also occur in SeMeCo and participate in the protective role of the self-generated exometabolome.

Finally, we would like to discuss the possible evolutionary implications of our results. It has so far been debated whether unicellular organisms would profit from a longer lifespan and if they have been selected for longevity.[84] Our study does not address this question directly, but it reveals an interesting new possibility that could be important in light of the high proportion of natural microbial communities containing auxotrophs.[22,67,85] Methionine auxotrophs are long-lived but require cells with a shorter lifespan to supply them with methionine. The glycerol excreted by the methionine consumers prolonged the lifespan of the methionine producers, indicating that the longer lifespan could provide a direct return benefit to the methionine consumers. Auxotrophy-prototrophy interactions might hence select for longevity of cells that provide essential metabolites to microbial communities. In any case, our results prompt future studies aiming at closely examining the exometabolome when lifespan extensions are reported, specifically when metabolic interventions such as metabolite restriction/supplementation or metabolism-modulating drug treatments are applied.

Limitations of the study

Metabolite exchange interactions are difficult to trace in wild-type cells, hence we have exploited the advantages of SeMeCo. In SeMeCo, a higher number of cells share histidine, leucine, uracil or methionine, but overall, being an auxotroph means the cells are less metabolically versatile, compared with prototrophic wild-type cells. SeMeCo will hence not capture all metabolic properties found in wild-type cells. Moreover, despite the fact that cells of the 16 metabotypes, that emerge from the segregation of the four metabolic markers used in our study diverge broadly in their metabolism,[43] the community allows us to monitor only a fraction of their possible metabolite exchange interactions. That means, methionine and glycerol will not be the only exometabolites impacting the aging process.

Secondly, lifespan experiments are conducted in batch culture, as typical in the field, and in yeast colonies, but the laboratory cultures will only approximate and reflect the aging process of cells within natural communities. We hope our results encourage the development of methods that would simplify the study of CLS-like aging phenotypes of cells that participate in natural communities.

STAR★METHODS

Detailed methods are provided in the online version of this paper and include the following:

- KEY RESOURCES TABLE
- RESOURCE AVAILABILITY
  - Lead contact
  - Materials availability
  - Data and code availability
- EXPERIMENTAL MODEL AND SUBJECT DETAILS
  - Yeast strain construction
- METHOD DETAILS
  - Yeast strains culture
  - Growth assays
  - Chronologic lifespan
  - Metabotyping
  - pH analysis
  - Oxygen consumption
  - Reactive Oxygen Species Levels
  - Targeted metabolomics
  - Genome-scale metabolic modelling (flux balance analysis)
- QUANTIFICATION AND STATISTICAL ANALYSIS

SUPPLEMENTAL INFORMATION

Supplemental information can be found online at https://doi.org/10.1016/j.cell.2022.12.007.

ACKNOWLEDGMENTS

We thank the Francis Crick Science and Technology Platforms (STP), specially Hefin Rhys, Sukhveer Purewal, and Ana Água-Doce from the Flow Cytometry STP; Paull Driscoll, Nathalie Legrave, and James Macrae from the Metabolomics STP; Teresa Higgins, Gareth Houghton-Brown, and Magdalena Sokalska from the Media STP for all the technical support and advice; and Hezi Tenemboim and our colleagues for critically reading the manuscript. This work was supported by the Francis Crick Institute, which receives its core funding from Cancer Research UK (FC001134), the UK Medical Research Council (FC001134), and the Wellcome Trust (FC001134), and received specific funding from the European Research Council (ERC) under grant agreement ERC-SyG-2020 951475 (to M.R.), the Wellcome Trust (IA 200829/Z/16/Z to M.R.),), the Ministry of Education and Research (BMBF), as part of the National Research Node "Mass spectrometry in Systems Medicine (MSCoreSys)", under grant agreements 031L0220 (to M.R.) and 161L0221 (to V.D.), and the European Commission (EC) as part of CoBioTech project Sycolim ID#33 (BMBF 161B0931) to MR supporting C.C.-M., S.K., M.M., C.B.M., P.T., S.J.T., S.J.V., A.F., B.M.H., L.H.-D., S.K.A., L.S., J.S.L.Y., V.D., and M.M. C.B.M. is also supported by the Precision Proteomics Center Davos that receives funding from the Swiss canton of Grisons. P.T. is also supported by funding from the European Union's Horizon 2020 research and innovation programme under the Marie Skłodowska-Curie grant agreement no 101026830. A.F. is also supported by the Life Science Stiftung (Charite 2019.01). M.T.A. is also supportedby the United Arab Emirates University, Al Ain, UAE (startup grant G00003688). R.T. is also supported by the National Research, Development and Innovation Office PD 128271; and B.P. is also supported by the National Research, Development and Innovation Office Élvonal Program KKP 129814, the "Lendület" program of the Hungarian Academy of Sciences LP2009-013/2012, and the European Union's Horizon 2020 research and innovation program grant no. 739593. A.Z. was also supported by the SciLifeLab funding and Marius Jason Jakulis (MJJ) foundation. For the purpose of Open Access, the author has applied a CC BY public copyright license to any Author Accepted Manuscript version arising from this submission.

AUTHOR CONTRIBUTIONS

Conceptualization, C.C.-M. and M.R.; methodology, C.C.-M., S.K., SJ.T., M.M., S.J.V., C.B.M, and V.D.; investigation, C.C.-M, S.K., R.T., C.B.M., M.M., S.J.V., A.F., K.C., L.H.-D., S.K.A., L.S., J.S.L.Y., and B.P.; formal analysis, C.C.-M., P.T., B.M.H., V.D., A.Z., S.J.T., and M.T.A.; writing – original draft, C.C.-M. and M.R.; writing – review & editing, C.C.-M. and M.R. with the support of all authors; funding acquisition, M.R.; supervision, C.C.-M. and M.R.

DECLARATION OF INTERESTS

K.C. is currently employed by AstraZeneca.

INCLUSION AND DIVERSITY

We support inclusive, diverse, and equitable conduct of research.

Received: March 22, 2022
Revised: September 7, 2022
Accepted: December 5, 2022
Published: January 5, 2023

REFERENCES

1. Zhu, J., and Thompson, C.B. (2019). Metabolic regulation of cell growth and proliferation. Nat. Rev. Mol. Cell Biol. *20*, 436–450. https://doi.org/10.1038/s41580-019-0123-5.
2. López-Otín, C., Galluzzi, L., Freije, J.M.P., Madeo, F., and Kroemer, G. (2016). Metabolic control of longevity. Cell *166*, 802–821. https://doi.org/10.1016/j.cell.2016.07.031.
3. Moretton, A., and Loizou, J.I. (2020). Interplay between cellular metabolism and the DNA damage response in cancer. Cancers *12*, 2051. https://doi.org/10.3390/cancers12082051.
4. Tan, B.L., Norhaizan, M.E., Liew, W.P., and Sulaiman Rahman, H. (2018). Antioxidant and oxidative stress: a mutual interplay in age-related diseases. Front. Pharmacol. *9*, 1162. https://doi.org/10.3389/fphar.2018.01162.
5. Balaban, R.S., Nemoto, S., and Finkel, T. (2005). Mitochondria, oxidants, and aging. Cell *120*, 483–495. https://doi.org/10.1016/j.cell.2005.02.001.
6. Kold-Christensen, R., and Johannsen, M. (2020). Methylglyoxal metabolism and aging-related disease: moving from correlation toward causation. Trends Endocrinol. Metab. *31*, 81–92. https://doi.org/10.1016/j.tem.2019.10.003.
7. Kapahi, P., Chen, D., Rogers, A.N., Katewa, S.D., Li, P.W.-L., Thomas, E.L., and Kockel, L. (2010). With TOR, less is more: a key role for the conserved nutrient-sensing TOR pathway in aging. Cell Metab. *11*, 453–465. https://doi.org/10.1016/j.cmet.2010.05.001.
8. Wang, Y.-P., and Lei, Q.-Y. (2018). Metabolite sensing and signaling in cell metabolism. Signal Transduct. Target. Ther. *3*, 30. https://doi.org/10.1038/s41392-018-0024-7.
9. Salminen, A., and Kaarniranta, K. (2012). AMP-activated protein kinase (AMPK) controls the aging process via an integrated signaling network. Ageing Res. Rev. *11*, 230–241. https://doi.org/10.1016/j.arr.2011.12.005.
10. Jang, C., Hui, S., Zeng, X., Cowan, A.J., Wang, L., Chen, L., Morscher, R.J., Reyes, J., Frezza, C., Hwang, H.Y., et al. (2019). Metabolite exchange between mammalian organs quantified in pigs. Cell Metab. *30*. 594–606.e3. https://doi.org/10.1016/j.cmet.2019.06.002.
11. Richter, F.C., Obba, S., and Simon, A.K. (2018). Local exchange of metabolites shapes immunity. Immunology *155*, 309–319. https://doi.org/10.1111/imm.12978.
12. Douglas, A.E. (2020). The microbial exometabolome: ecological resource and architect of microbial communities. Philos. Trans. R. Soc. Lond. B Biol. Sci. *375*. 20190250. https://doi.org/10.1098/rstb.2019.0250.
13. D'Souza, G., Shitut, S., Preussger, D., Yousif, G., Waschina, S., and Kost, C. (2018). Ecology and evolution of metabolic cross-feeding interactions in bacteria. Nat. Prod. Rep. *35*, 455–488. https://doi.org/10.1039/c8np00009c.
14. Campbell, K., Herrera-Dominguez, L., Correia-Melo, C., Zelezniak, A., and Ralser, M. (2018). Biochemical principles enabling metabolic cooperativity and phenotypic heterogeneity at the single cell level. Curr. Opin. Syst. Biol. *8*, 97–108. https://doi.org/10.1016/j.coisb.2017.12.001.
15. Paczia, N., Nilgen, A., Lehmann, T., Gätgens, J., Wiechert, W., and Noack, S. (2012). Extensive exometabolome analysis reveals extended overflow metabolism in various microorganisms. Microb. Cell Factories *11*, 122. https://doi.org/10.1186/1475-2859-11-122.
16. Vazquez, A., and Oltvai, Z.N. (2016). Macromolecular crowding explains overflow metabolism in cells. Sci. Rep. *6*, 31007. https://doi.org/10.1038/srep31007.
17. Yamagishi, J.F., Saito, N., and Kaneko, K. (2021). Adaptation of metabolite leakiness leads to symbiotic chemical exchange and to a resilient microbial ecosystem. PLoS Comput. Biol. *17*. e1009143. https://doi.org/10.1371/journal.pcbi.1009143.
18. Conrad, M., Schothorst, J., Kankipati, H.N., Van Zeebroeck, G., Rubio-Texeira, M., and Thevelein, J.M. (2014). Nutrient sensing and signaling in the yeast Saccharomyces cerevisiae. FEMS Microbiol. Rev. *38*, 254–299. https://doi.org/10.1111/1574-6976.12065.
19. Goyal, S., Yuan, J., Chen, T., Rabinowitz, J.D., and Wingreen, N.S. (2010). Achieving optimal growth through product feedback inhibition

in metabolism. PLoS Comput. Biol. *6*. e1000802. https://doi.org/10.1371/journal.pcbi.1000802.

20. Smith, P., and Schuster, M. (2019). Public goods and cheating in microbes. Curr. Biol. *29*, R442–R447. https://doi.org/10.1016/j.cub.2019.03.001.
21. Olin-Sandoval, V., Yu, J.S.L., Miller-Fleming, L., Alam, M.T., Kamrad, S., Correia-Melo, C., Haas, R., Segal, J., Peña Navarro, D.A., Herrera-Dominguez, L., et al. (2019). Lysine harvesting is an antioxidant strategy and triggers underground polyamine metabolism. Nature *572*, 249–253. https://doi.org/10.1038/s41586-019-1442-6.
22. Yu, J.S.L., Correia-Melo, C., Zorrilla, F., Herrera-Dominguez, L., Wu, M.Y., Hartl, J., Campbell, K., Blasche, S., Kreidl, M., Egger, A.-S., et al. (2022). Microbial communities form rich extracellular metabolomes that foster metabolic interactions and promote drug tolerance. Nat. Microbiol. *7*, 542–555. https://doi.org/10.1038/s41564-022-01072-5.
23. Powers, R.W., 3rd, Kaeberlein, M., Caldwell, S.D., Kennedy, B.K., and Fields, S. (2006). Extension of chronological life span in yeast by decreased TOR pathway signaling. Genes Dev. *20*, 174–184. https://doi.org/10.1101/gad.1381406.
24. Howitz, K.T., Bitterman, K.J., Cohen, H.Y., Lamming, D.W., Lavu, S., Wood, J.G., Zipkin, R.E., Chung, P., Kisielewski, A., Zhang, L.-L., et al. (2003). Small molecule activators of sirtuins extend Saccharomyces cerevisiae lifespan. Nature *425*, 191–196. https://doi.org/10.1038/nature01960.
25. Kennedy, B.K., Austriaco, N.R., Zhang, J., and Guarente, L. (1995). Mutation in the silencing gene SIR4 can delay aging in S. cerevisiae. Cell *80*, 485–496. https://doi.org/10.1016/0092-8674(95)90499-9.
26. Lu, J.-Y., Lin, Y.-Y., Sheu, J.-C., Wu, J.-T., Lee, F.-J., Chen, Y., Lin, M.-I., Chiang, F.-T., Tai, T.-Y., Berger, S.L., et al. (2011). Acetylation of yeast AMPK controls intrinsic aging independently of caloric restriction. Cell *146*, 969–979. https://doi.org/10.1016/j.cell.2011.07.044.
27. MacLean, M., Harris, N., and Piper, P.W. (2001). Chronological lifespan of stationary phase yeast cells; a model for investigating the factors that might influence the ageing of postmitotic tissues in higher organisms. Yeast *18*, 499–509. https://doi.org/10.1002/yea.701.
28. Campbell, K., Vowinckel, J., Mülleder, M., Malmsheimer, S., Lawrence, N., Calvani, E., Miller-Fleming, L., Alam, M.T., Christen, S., Keller, M.A., and Ralser, M. (2015). Self-establishing communities enable cooperative metabolite exchange in a eukaryote. eLife *4*, e09943. https://doi.org/10.7554/eLife.09943.
29. Brachmann, C.B., Davies, A., Cost, G.J., Caputo, E., Li, J., Hieter, P., and Boeke, J.D. (1998). Designer deletion strains derived from Saccharomyces cerevisiae S288C: a useful set of strains and plasmids for PCR-mediated gene disruption and other applications. Yeast *14*, 115–132.
30. Wickerham, L.J. (1951). Taxonomy of Yeasts (U.S. Dept. of Agriculture).
31. Kamrad, S., Grossbach, J., Rodríguez-López, M., Mülleder, M., Townsend, S., Cappelletti, V., Stojanovski, G., Correia-Melo, C., Picotti, P., Beyer, A., et al. (2020). Pyruvate kinase variant of fission yeast tunes carbon metabolism, cell regulation, growth and stress resistance. Mol. Syst. Biol. *16*, e9270. https://doi.org/10.15252/msb.20199270.
32. Galdieri, L., Mehrotra, S., Yu, S., and Vancura, A. (2010). Transcriptional regulation in yeast during diauxic shift and stationary phase. Omics *14*, 629–638. https://doi.org/10.1089/omi.2010.0069.
33. Slavov, N., and Botstein, D. (2011). Coupling among growth rate response, metabolic cycle, and cell division cycle in yeast. Mol. Biol. Cell *22*, 1997–2009. https://doi.org/10.1091/mbc.E11-02-0132.
34. Zampar, G.G., Kümmel, A., Ewald, J., Jol, S., Niebel, B., Picotti, P., Aebersold, R., Sauer, U., Zamboni, N., and Heinemann, M. (2013). Temporal system-level organization of the switch from glycolytic to gluconeogenic operation in yeast. Mol. Syst. Biol. *9*, 651. https://doi.org/10.1038/msb.2013.11.
35. Bianchi, F., van't Klooster, J.S., Ruiz, S.J., and Poolman, B. (2019). Regulation of amino acid transport in Saccharomyces cerevisiae. Microbiol. Mol. Biol. Rev. *83*. e00024-19. https://doi.org/10.1128/MMBR.00024-19.
36. Kumar, K., Venkatraman, V., and Bruheim, P. (2021). Adaptation of central metabolite pools to variations in growth rate and cultivation conditions in Saccharomyces cerevisiae. Microb. Cell Factories *20*, 64. https://doi.org/10.1186/s12934-021-01557-8.
37. Ponomarova, O., Gabrielli, N., Sévin, D.C., Mülleder, M., Zirngibl, K., Bulyha, K., Andrejev, S., Kafkia, E., Typas, A., Sauer, U., et al. (2017). Yeast creates a niche for symbiotic lactic acid bacteria through nitrogen overflow. Cell Syst. *5*. 345–357.e6. https://doi.org/10.1016/j.cels.2017.09.002.
38. Mülleder, M., Bluemlein, K., and Ralser, M. (2017). A high-throughput method for the quantitative determination of free amino acids in Saccharomyces cerevisiae by hydrophilic interaction chromatography-tandem mass spectrometry. Cold Spring Harb. Protoc. *2017*. pdb.prot089094. https://doi.org/10.1101/pdb.prot089094.
39. Campbell, K., Correia-Melo, C., and Ralser, M. (2019). Self-establishing communities: a yeast model to study the physiological impact of metabolic cooperation in eukaryotic cells. Methods Mol. Biol. *2049*, 263–282. https://doi.org/10.1007/978-1-4939-9736-7_16.
40. Shou, W., Ram, S., and Vilar, J.M.G. (2007). Synthetic cooperation in engineered yeast populations. Proc. Natl. Acad. Sci. USA *104*, 1877–1882. https://doi.org/10.1073/pnas.0610575104.
41. Váchová, L., Cáp, M., and Palková, Z. (2012). Yeast colonies: a model for studies of aging, environmental adaptation, and longevity. Oxid. Med. Cell. Longev. *2012*, 601836. https://doi.org/10.1155/2012/601836.
42. Burtner, C.R., Murakami, C.J., Kennedy, B.K., and Kaeberlein, M. (2009). A molecular mechanism of chronological aging in yeast. Cell Cycle *8*, 1256–1270. https://doi.org/10.4161/cc.8.8.8287.
43. Alam, M.T., Zelezniak, A., Mülleder, M., Shliaha, P., Schwarz, R., Capuano, F., Vowinckel, J., Radmanesfahar, E., Krüger, A., Calvani, E., et al. (2016). The metabolic background is a global player in Saccharomyces gene expression epistasis. Nat. Microbiol. *1*, 15030. https://doi.org/10.1038/nmicrobiol.2015.30.
44. Bárcena, C., Quirós, P.M., Durand, S., Mayoral, P., Rodríguez, F., Caravia, X.M., Mariño, G., Garabaya, C., Fernández-García, M.T., Kroemer, G., et al. (2018). Methionine restriction extends lifespan in progeroid mice and alters lipid and bile acid metabolism. Cell Rep. *24*, 2392–2403. https://doi.org/10.1016/j.celrep.2018.07.089.
45. Lee, B.C., Kaya, A., Ma, S., Kim, G., Gerashchenko, M.V., Yim, S.H., Hu, Z., Harshman, L.G., and Gladyshev, V.N. (2014). Methionine restriction extends lifespan of Drosophila melanogaster under conditions of low amino-acid status. Nat. Commun. *5*, 3592. https://doi.org/10.1038/ncomms4592.
46. Plummer, J.D., and Johnson, J.E. (2019). Extension of cellular lifespan by methionine restriction involves alterations in central carbon metabolism and is mitophagy-dependent. Front. Cell Dev. Biol. *7*, 301. https://doi.org/10.3389/fcell.2019.00301.
47. Brind, J., Malloy, V., Augie, I., Caliendo, N., Vogelman, J.H., Zimmerman, J.A., and Orentreich, N. (2011). Dietary glycine supplementation mimics lifespan extension by dietary methionine restriction in Fisher 344 rats. FASEB J. *25*, 528.2. https://doi.org/10.1096/fasebj.25.1_supplement.528.2.
48. Ruckenstuhl, C., Netzberger, C., Entfellner, I., Carmona-Gutierrez, D., Kickenweiz, T., Stekovic, S., Gleixner, C., Schmid, C., Klug, L., Sorgo, A.G., et al. (2014). Lifespan extension by methionine restriction requires autophagy-dependent vacuolar acidification. PLoS Genet. *10*. e1004347. https://doi.org/10.1371/journal.pgen.1004347.
49. Orentreich, N., Matias, J.R., DeFelice, A., and Zimmerman, J.A. (1993). Low methionine ingestion by rats extends life span. J. Nutr. *123*, 269–274. https://doi.org/10.1093/jn/123.2.269.
50. Piper, P.W. (2006). Long-lived yeast as a model for ageing research. Yeast *23*, 215–226. https://doi.org/10.1002/yea.1354.

51. Metcalfe, N.B., and Monaghan, P. (2003). Growth versus lifespan: perspectives from evolutionary ecology. Exp. Gerontol. *38*, 935–940. https://doi.org/10.1016/s0531-5565(03)00159-1.

52. Machado, D., Maistrenko, O.M., Andrejev, S., Kim, Y., Bork, P., Patil, K.R., and Patil, K.R. (2021). Polarization of microbial communities between competitive and cooperative metabolism. Nat. Ecol. Evol. *5*, 195–203. https://doi.org/10.1038/s41559-020-01353-4.

53. Thompson, L.R., Sanders, J.G., McDonald, D., Amir, A., Ladau, J., Locey, K.J., Prill, R.J., Tripathi, A., Gibbons, S.M., Ackermann, G., et al. (2017). A communal catalogue reveals Earth's multiscale microbial diversity. Nature *551*, 457–463. https://doi.org/10.1038/nature24621.

54. Muenzner, J., Trébulle, P., Agostini, F., Messner, C.B., Steger, M., Lehmann, A., Caudal, E., Egger, A.-S., Amari, F., Barthel, N., et al. (2022). The natural diversity of the yeast proteome reveals chromosome-wide dosage compensation in aneuploids https://doi.org/10.1101/2022.04.06.487392.

55. Peter, J., De Chiara, M., Friedrich, A., Yue, J.-X., Pflieger, D., Bergström, A., Sigwalt, A., Barre, B., Freel, K., Llored, A., et al. (2018). Genome evolution across 1,011 Saccharomyces cerevisiae isolates. Nature *556*, 339–344. https://doi.org/10.1038/s41586-018-0030-5.

56. Čáp, M., Štěpánek, L., Harant, K., Váchová, L., and Palková, Z. (2012). Cell differentiation within a yeast colony: metabolic and regulatory parallels with a tumor-affected organism. Mol. Cell *46*, 436–448. https://doi.org/10.1016/j.molcel.2012.04.001.

57. Vowinckel, J., Zelezniak, A., Bruderer, R., Mülleder, M., Reiter, L., and Ralser, M. (2018). Cost-effective generation of precise label-free quantitative proteomes in high-throughput by microLC and data-independent acquisition. Sci. Rep. *8*, 4346. https://doi.org/10.1038/s41598-018-22610-4.

58. Demichev, V., Messner, C.B., Vernardis, S.I., Lilley, K.S., and Ralser, M. (2020). DIA-NN: neural networks and interference correction enable deep proteome coverage in high throughput. Nat. Methods *17*, 41–44. https://doi.org/10.1038/s41592-019-0638-x.

59. de Godoy, L.M.F., Olsen, J.V., Cox, J., Nielsen, M.L., Hubner, N.C., Fröhlich, F., Walther, T.C., and Mann, M. (2008). Comprehensive mass-spectrometry-based proteome quantification of haploid versus diploid yeast. Nature *455*, 1251–1254. https://doi.org/10.1038/nature07341.

60. Darzi, Y., Letunic, I., Bork, P., and Yamada, T. (2018). iPath3.0: interactive pathways explorer v3. Nucleic Acids Res. *46*, W510–W513. https://doi.org/10.1093/nar/gky299.

61. Lin, S.J., Kaeberlein, M., Andalis, A.A., Sturtz, L.A., Defossez, P.-A., Culotta, V.C., Fink, G.R., and Guarente, L. (2002). Calorie restriction extends Saccharomyces cerevisiae lifespan by increasing respiration. Nature *418*, 344–348. https://doi.org/10.1038/nature00829.

62. Orlandi, I., Ronzulli, R., Casatta, N., and Vai, M. (2013). Ethanol and acetate acting as carbon/energy sources negatively affect yeast chronological aging. Oxid. Med. Cell. Longev. *2013*, 802870. https://doi.org/10.1155/2013/802870.

63. Wei, M., Fabrizio, P., Madia, F., Hu, J., Ge, H., Li, L.M., and Longo, V.D. (2009). Tor1/Sch9-regulated carbon source substitution is as effective as calorie restriction in life span extension. PLoS Genet. *5*. e1000467. https://doi.org/10.1371/journal.pgen.1000467.

64. Parkhitko, A.A., Jouandin, P., Mohr, S.E., and Perrimon, N. (2019). Methionine metabolism and methyltransferases in the regulation of aging and lifespan extension across species. Aging Cell *18*, e13034. https://doi.org/10.1111/acel.13034.

65. Minois, N., Carmona-Gutierrez, D., and Madeo, F. (2011). Polyamines in aging and disease. Aging *3*, 716–732. https://doi.org/10.18632/aging.100361.

66. Molon, M., Woznicka, O., and Zebrowski, J. (2018). Cell wall biosynthesis impairment affects the budding lifespan of the Saccharomyces cerevisiae yeast. Biogerontology *19*, 67–79. https://doi.org/10.1007/s10522-017-9740-6.

67. Zelezniak, A., Andrejev, S., Ponomarova, O., Mende, D.R., Bork, P., and Patil, K.R. (2015). Metabolic dependencies drive species co-occurrence in diverse microbial communities. Proc. Natl. Acad. Sci. USA. *112*, 6449–6454. https://doi.org/10.1073/pnas.1421834112.

68. Kouzuma, A., Kato, S., and Watanabe, K. (2015). Microbial interspecies interactions: recent findings in syntrophic consortia. Front. Microbiol. *6*, 477. https://doi.org/10.3389/fmicb.2015.00477.

69. Kundu, P., Manna, B., Majumder, S., and Ghosh, A. (2019). Species-wide metabolic interaction network for understanding natural lignocellulose digestion in termite gut microbiota. Sci. Rep. *9*, 16329. https://doi.org/10.1038/s41598-019-52843-w.

70. Skandamis, P.N., and Jeanson, S. (2015). Colonial vs. planktonic type of growth: mathematical modeling of microbial dynamics on surfaces and in liquid, semi-liquid and solid foods. Front. Microbiol. *6*, 1178. https://doi.org/10.3389/fmicb.2015.01178.

71. Brosnan, J.T., and Brosnan, M.E. (2006). The sulfur-containing amino acids: an overview. J. Nutr. *136* (*Suppl*). 1636S –1640S. https://doi.org/10.1093/jn/136.6.1636S.

72. Dong, Z., Sinha, R., and Richie, J.P., Jr. (2018). Disease prevention and delayed aging by dietary sulfur amino acid restriction: translational implications. Ann. NY Acad. Sci. *1418*, 44–55. https://doi.org/10.1111/nyas.13584.

73. Sanderson, S.M., Gao, X., Dai, Z., and Locasale, J.W. (2019). Methionine metabolism in health and cancer: a nexus of diet and precision medicine. Nat. Rev. Cancer *19*, 625–637. https://doi.org/10.1038/s41568-019-0187-8.

74. Gao, X., Sanderson, S.M., Dai, Z., Reid, M.A., Cooper, D.E., Lu, M., Richie, J.P., Jr., Ciccarella, A., Calcagnotto, A., Mikhael, P.G., et al. (2019). Dietary methionine influences therapy in mouse cancer models and alters human metabolism. Nature *572*, 397–401. https://doi.org/10.1038/s41586-019-1437-3.

75. Udom, N., Chansongkrow, P., Charoensawan, V., and Auesukaree, C. (2019). Coordination of the cell wall integrity and high-osmolarity glycerol pathways in response to ethanol stress in Saccharomyces cerevisiae. Appl. Environ. Microbiol. *85*. e00551-19. https://doi.org/10.1128/AEM.00551-19.

76. Aung, H.W., Henry, S.A., and Walker, L.P. (2013). Revising the representation of fatty acid, glycerolipid, and glycerophospholipid metabolism in the consensus model of yeast metabolism. Ind. Biotechnol. (New Rochelle NY) *9*, 215–228. https://doi.org/10.1089/ind.2013.0013.

77. Werner-Washburne, M., Braun, E., Johnston, G.C., and Singer, R.A. (1993). Stationary phase in the yeast Saccharomyces cerevisiae. Microbiol. Rev. *57*, 383–401. https://doi.org/10.1128/mr.57.2.383-401.1993.

78. Uthus, E.O., and Brown-Borg, H.M. (2003). Altered methionine metabolism in long living Ames dwarf mice. Exp. Gerontol. *38*, 491–498. https://doi.org/10.1016/s0531-5565(03)00008-1.

79. Cao, X., Ding, L., Xie, Z.Z., Yang, Y., Whiteman, M., Moore, P.K., and Bian, J.S. (2019). A review of hydrogen sulfide synthesis, metabolism, and measurement: is modulation of hydrogen sulfide a novel therapeutic for cancer? Antioxid. Redox Signal. *31*, 1–38. https://doi.org/10.1089/ars.2017.7058.

80. Hine, C., Harputlugil, E., Zhang, Y., Ruckenstuhl, C., Lee, B.C., Brace, L., Longchamp, A., Treviño-Villarreal, J.H., Mejia, P., Ozaki, C.K., et al. (2015). Endogenous hydrogen sulfide production is essential for dietary restriction benefits. Cell *160*, 132–144. https://doi.org/10.1016/j.cell.2014.11.048.

81. Hine, C., Zhu, Y., Hollenberg, A.N., and Mitchell, J.R. (2018). Dietary and endocrine regulation of endogenous hydrogen sulfide production: implications for longevity. Antioxid. Redox Signal. *28*, 1483–1502. https://doi.org/10.1089/ars.2017.7434.

82. Shah, A.A., Liu, B., Tang, Z., Wang, W., Yang, W., Hu, Q., Liu, Y., Zhang, N., and Liu, K. (2021). Hydrogen sulfide treatment at the late growth stage

of Saccharomyces cerevisiae extends chronological lifespan. Aging *13*, 9859–9873. https://doi.org/10.18632/aging.202738.

83. Yu, J.S.L., Heineike, B.M., Hartl, J., Correia-Melo, C., Aulakh, S.K., Lehmann, A., Lemke, O., Agostini, F., Lee, C.T., Demichev, V., et al. (2022). Inorganic sulfur fixation via a new homocysteine synthase allows yeast cells to cooperatively compensate for methionine auxotrophy. PLoS Biol. https://doi.org/10.1371/journal.pbio.3001912.
84. Moger-Reischer, R.Z., and Lennon, J.T. (2019). Microbial ageing and longevity. Nat. Rev. Microbiol. *17*, 679–690. https://doi.org/10.1038/s41579-019-0253-y.
85. Zengler, K., and Zaramela, L.S. (2018). The social network of microorganisms - how auxotrophies shape complex communities. Nat. Rev. Microbiol. *16*, 383–390. https://doi.org/10.1038/s41579-018-0004-5.
86. Perez-Riverol, Y., Bai, J., Bandla, C., García-Seisdedos, D., Hewapathirana, S., Kamatchinathan, S., Kundu, D.J., Prakash, A., Frericks-Zipper, A., Eisenacher, M., et al. (2022). The PRIDE database resources in 2022: a hub for mass spectrometry-based proteomics evidences. Nucleic Acids Res. *50*, D543–D552. https://doi.org/10.1093/nar/gkab1038.
87. Mülleder, M., Campbell, K., Matsarskaia, O., Eckerstorfer, F., and Ralser, M. (2016). Saccharomyces cerevisiae single-copy plasmids for auxotrophy compensation, multiple marker selection, and for designing metabolically cooperating communities. F1000Res *5*, 2351. https://doi.org/10.12688/f1000research.9606.1.
88. Gietz, R.D., and Schiestl, R.H. (2007). High-efficiency yeast transformation using the LiAc/SS carrier DNA/PEG method. Nat. Protoc. *2*, 31–34. https://doi.org/10.1038/nprot.2007.13.
89. Sprouffske, K., and Wagner, A. (2016). Growthcurver: an R package for obtaining interpretable metrics from microbial growth curves. BMC Bioinformatics *17*, 172. https://doi.org/10.1186/s12859-016-1016-7.
90. Longo, V.D., Shadel, G.S., Kaeberlein, M., and Kennedy, B. (2012). Replicative and chronological aging in Saccharomyces cerevisiae. Cell Metab. *16*, 18–31. https://doi.org/10.1016/j.cmet.2012.06.002.
91. Romila, C.A., Townsend, S., Malecki, M., Kamrad, S., Rodríguez-López, M., Hillson, O., Cotobal, C., Ralser, M., and Bähler, J. (2021). Barcode sequencing and a high-throughput assay for chronological lifespan uncover ageing-associated genes in fission yeast. Microb. Cell *8*, 146–160. https://doi.org/10.1101/2021.03.04.433786.
92. Kamrad, S., Rodríguez-López, M., Cotobal, C., Correia-Melo, C., Ralser, M., and Bähler, J. (2020). Pyphe, a python toolbox for assessing microbial growth and cell viability in high-throughput colony screens. eLife *9*, e55160. https://doi.org/10.7554/eLife.55160.
93. Ewald, J.C., Heux, S., and Zamboni, N. (2009). High-throughput quantitative metabolomics: workflow for cultivation, quenching, and analysis of yeast in a multiwell format. Anal. Chem. *81*, 3623–3629. https://doi.org/10.1021/ac900002u.
94. Bligh, E.G., and Dyer, W.J. (1959). A rapid method of total lipid extraction and purification. Can. J. Biochem. Physiol. *37*, 911–917. https://doi.org/10.1139/o59-099.
95. Wong, J.M., Malec, P.A., Mabrouk, O.S., Ro, J., Dus, M., and Kennedy, R.T. (2016). Benzoyl chloride derivatization with liquid chromatography-mass spectrometry for targeted metabolomics of neurochemicals in biological samples. J. Chromatogr. A *1446*, 78–90. https://doi.org/10.1016/j.chroma.2016.04.006.
96. Messner, C.B., Demichev, V., Bloomfield, N., Yu, J.S.L., White, M., Kreidl, M., Egger, A.-S., Freiwald, A., Ivosev, G., Wasim, F., et al. (2021). Ultra-fast proteomics with Scanning SWATH. Nat. Biotechnol. *39*, 846–854. https://doi.org/10.1038/s41587-021-00860-4.
97. R Core Team (2015). R: a language and environment for statistical computing (R Foundation for Statistical Computing).
98. Cherry, J.M., Hong, E.L., Amundsen, C., Balakrishnan, R., Binkley, G., Chan, E.T., Christie, K.R., Costanzo, M.C., Dwight, S.S., Engel, S.R., et al. (2012). Saccharomyces Genome Database: the genomics resource of budding yeast. Nucleic Acids Res. *40*, D700–D705. https://doi.org/10.1093/nar/gkr1029.
99. Mo, M.L., Palsson, B.O., and Herrgård, M.J. (2009). Connecting extracellular metabolomic measurements to intracellular flux states in yeast. BMC Syst. Biol. *3*, 37.
100. Szappanos, B., Kovács, K., Szamecz, B., Honti, F., Costanzo, M., Baryshnikova, A., Gelius-Dietrich, G., Lercher, M.J., Jelasity, M., Myers, C.L., et al. (2011). An integrated approach to characterize genetic interaction networks in yeast metabolism. Nat. Genet. *43*, 656–662.
101. Heirendt, L., Arreckx, S., Pfau, T., Mendoza, S.N., Richelle, A., Heinken, A., Haraldsdóttir, H.S., Wachowiak, J., Keating, S.M., Vlasov, V., et al. (2019). Creation and analysis of biochemical constraint-based models using the COBRA Toolbox v.3.0. Nat. Protoc. *14*, 639–702. https://doi.org/10.1038/s41596-018-0098-2.
102. Kanehisa, M., Sato, Y., Kawashima, M., Furumichi, M., and Tanabe, M. (2016). KEGG as a reference resource for gene and protein annotation. Nucleic Acids Res. *44*, D457–D462. https://doi.org/10.1093/nar/gkv1070.
103. Ritchie, M.E., Phipson, B., Wu, D., Hu, Y., Law, C.W., Shi, W., and Smyth, G.K. (2015). limma powers differential expression analyses for RNA-sequencing and microarray studies. Nucleic Acids Res. *43*, e47. https://doi.org/10.1093/nar/gkv007.
104. Grüning, N.-M., and Ralser, M. (2021). Glycolysis: how a 300 yr long research journey that started with the desire to improve alcoholic beverages kept revolutionizing biochemistry. Curr. Opin. Syst. Biol. *28*, 100380. https://doi.org/10.1016/j.coisb.2021.100380.

STAR★METHODS

KEY RESOURCES TABLE

REAGENT or RESOURCE	SOURCE	IDENTIFIER
Chemicals, peptides, and recombinant proteins		
Bacto Dehydrated Agar	ThermoFisher Scientific	Cat# 214010
Bacto Peptone	ThermoFisher Scientific	Cat# 211677
Bacto Yeast Extract	ThermoFisher Scientific	Cat# 212750
D-Glucose (^{12}C-glucose)	Sigma-Aldrich	Cat# G8270
D-Glucose (^{13}C-glucose)	Sigma-Aldrich	Cat# 389374
Glycerol	Sigma-Aldrich	Cat# G2025
L-Histidine	Sigma-Aldrich	Cat# H8000
L-Leucine	Sigma-Aldrich	Cat# L8000
L-Methionine	Sigma-Aldrich	Cat# 64319
Uracil	Sigma-Aldrich	Cat# U0750
Yeast Nitrogen Base Without Amino Acids	Sigma-Aldrich	Cat# Y0626
Yeast Synthetic Drop-out Medium Supplements, without lysine	Sigma-Aldrich	Cat# Y1896
Acetonitrile (Optima LC-MS Grade, Fisher Chemical)	Fisher Scientific	Cat# A955-500
Acetic Acid (Eluent additive for LC-MS)	Honeywell Research Chemicals	Cat# 49199
Ammonium Bicarbonate (Eluent additive for LC-MS)	Sigma-Aldrich	Cat# 40867
Ammonium Formate (eluent additive for UHPLC-MS, Fluka)	Honeywell Research Chemicals	Cat#14266
DL-Dithiothreitol (BioUltra)	Sigma-Aldrich	Cat# 43815
Formic Acid (TraceSELECT, for trace analysis, Fluka)	Honeywell Research Chemicals	Cat# 06454
Iodoacetamide (BioUltra)	Sigma-Aldrich	Cat# I1149
Methanol (Optima LC-MS Grade, Fisher Chemical)	Fisher Scientific	Cat# A456-212
Trypsin (Sequence grade)	Promega	Cat# V511X
Urea (puriss. P.a., reag. Ph. Eur.)	Honeywell Research Chemicals	Cat# 33247H
Water (Optima LC-MS Grade, Fisher Chemical)	Fisher Scientific	Cat# W6500
LC-MS Standard amino acid: Alanine	Sigma-Aldrich	Cat# A7627
LC-MS Standard amino acid: Arginine	Sigma-Aldrich	Cat# A5131
LC-MS Standard amino acid: Asparagine	Sigma-Aldrich	Cat# A0884
LC-MS Standard amino acid: Aspartate	Sigma-Aldrich	Cat# A9256
LC-MS Standard amino acid: Glutamate	Sigma-Aldrich	Cat# G1251
LC-MS Standard amino acid: Glutamine	Sigma-Aldrich	Cat# G3126
LC-MS Standard amino acid: Glycine	Sigma-Aldrich	Cat# G7126
LC-MS Standard amino acid: Histidine	Sigma-Aldrich	Cat# H8125
LC-MS Standard amino acid: Isoleucine	Sigma-Aldrich	Cat# I2752
LC-MS Standard amino acid: Leucine	Sigma-Aldrich	Cat# L8000
LC-MS Standard amino acid: Lysine	Sigma-Aldrich	Cat# L5501
LC-MS Standard amino acid: Methionine	Sigma-Aldrich	Cat# M9625
LC-MS Standard amino acid: Phenylalanine	Sigma-Aldrich	Cat# P2126
LC-MS Standard amino acid: Proline	Sigma-Aldrich	Cat# P0380
LC-MS Standard amino acid: Serine	Sigma-Aldrich	Cat# S4500

(*Continued on next page*)

Continued

REAGENT or RESOURCE	SOURCE	IDENTIFIER
LC-MS Standard amino acid: Threonine	Sigma-Aldrich	Cat# T8625
LC-MS Standard amino acid: Tryptophan	Sigma-Aldrich	Cat# T0254
LC-MS Standard amino acid: Tyrosine	Sigma-Aldrich	Cat# T3754
LC-MS Standard amino acid: Valine	Sigma-Aldrich	Cat# V0500
LC-MS Standard nucleobase: Uracil	Sigma-Aldrich	Cat# U0750
LC-MS Standard nucleotide: Adenosine 5′-triphosphate (ATP)	Abcam	Cat# ab146562
LC-MS Standard nucleotide: Cytidine-5′-triphosphate (CTP)	Abcam	Cat# ab146217
LC-MS Standard nucleotide: Uridine-5′-triphosphate (UTP)	Abcam	Cat# ab146222
LC-MS Standard nucleotide: Guanosine-5′-triphosphate (GTP)	Abcam	Cat# ab146561
LC-MS Standard glycolytic intermediate: Glucose 6-phosphate	Sigma-Aldrich	Cat# G7879
LC-MS Standard glycolytic intermediate: Fructose 6-phosphate	Sigma-Aldrich	Cat# F3627
LC-MS Standard glycolytic intermediate: Glyceraldehyde 3-phosphate	Sigma-Aldrich	Cat# G5251
LC-MS Standard glycolytic intermediate: Dihydroxyacetone phosphate	Sigma-Aldrich	Cat# 37442
LC-MS Standard glycolytic intermediate: Phosphoenolpyruvic acid	Sigma-Aldrich	Cat# P7127
LC-MS Standard TCA intermediate: Citric acid	Sigma-Aldrich	Cat# W302600
LC-MS Standard TCA intermediate: *Cis*-aconitic acid	Sigma-Aldrich	Cat# A3412
LC-MS Standard TCA intermediate: Alpha-ketoglutaric acid	Sigma-Aldrich	Cat# 75892
LC-MS Standard TCA intermediate: Succinic acid	Sigma-Aldrich	Cat# S3674
LC-MS Standard TCA intermediate: Fumaric acid	Sigma-Aldrich	Cat# 47910
LC-MS Standard TCA intermediate: Malic acid	Sigma-Aldrich	Cat# 27606
LC-MS Standard glutathione: Glutathione	Sigma-Aldrich	Cat# G6013
LC-MS Standard glutathione: Glutathione disulphide	Sigma-Aldrich	Cat# G4376
LC-MS 13C Standards: Algal lyophilised cells-13C (Synechococcus sp.)	Sigma-Aldrich	Cat# 487945
LC-MS Standards polyamines: putrescine, spermidine, spermine	Sigma-Aldrich	Cat# 51799, S2626, S3256
HPLC Standard: Ethanol	WVR	Cat# 153385E
HPLC Standard: Glycerol	WVR	Cat# 24386.298
HPLC Standard: Sodium acetate	Sigma-Aldrich	Cat# S7670-250G
Pyridine	Honeywell	Cat# 360-570
Sodium carbonate	Sigma-Aldrich	Cat# 223530
Benzoyl chloride	Alfa Aesar	Cat# A14107
Sulfuric acid	Applichem	Cat# 141085.1211
Formaldehyde 37% solution	Sigma-Aldrich	Cat# F1635
Chloroform	J.T. Baker	Cat# 7386.1000
Critical commercial assays		
LIVE/DEAD Fixable Far Red Dead Cell Stain Kit, for 633 or 635 nm excitation, Invitrogen	ThermoFisher Scientific	Cat# L10120
Dihydrorhodamine 123 (DHR), Invitrogen	ThermoFisher Scientific	Cat# D23806
Deposited data		
SeMeCo aging proteome dataset	This study	PRIDE Project accession: PXD036444.
Wild-type yeast supplemented with/out amino acids proteome dataset	This study	Mendeley Data: https://doi.org/10.17632/sd8zthmrk4.1.

(*Continued on next page*)

Continued

REAGENT or RESOURCE	SOURCE	IDENTIFIER
1k wild yeast isolates collection proteome dataset	Muenzner et al.[54]	N/A
EMP prokaryotic natural auxotrophic species dataset	Machado et al.[52]	https://github.com/cdanielmachado/cooccurrence/blob/master/download.sh
Experimental models: Organisms/strains		
S.cerevisiae, BY4741; (MATa: his3Δ1, leu2Δ0, ura3Δ0, met15Δ0)	ATCC	https://www.atcc.org/
S.cerevisiae, BY4741: Prototrophic; (MATa: *HIS3, LEU2, URA3, MET15)*	Olin-Sandoval et al.[21]	N/A
S.cerevisiae, BY4741: SeMeCo; (MATa: p*HIS3,* p*LEU2,* p*URA3,* p*MET15)*	Yu et al.[22]	N/A
S.cerevisiae, BY4741: *HIS3*-SeMeCo; (MATa: *HIS3,* p*LEU2,* p*URA3,* p*MET15)*	This study	N/A
S.cerevisiae, BY4741: *LEU2*-SeMeCo; (MATa: *LEU2,* p*HIS3,* p*URA3,* p*MET15)*	This study	N/A
S.cerevisiae, BY4741: *URA3*-SeMeCo; (MATa: *URA3,* p*HIS3,* p*LEU2,* p*MET15)*	This study	N/A
S.cerevisiae, BY4741: *MET15*-SeMeCo; (MATa: *MET15,* p*HIS3,* p*LEU2,* p*URA3)*	This study	N/A
S.cerevisiae, BY4741: *met15*Δ; (MATa: *met15*Δ0, *HIS3, LEU2, URA3*)	This study	N/A
S.cerevisiae, BY4741: pM-SeMeCo; (MATa: *his3*Δ1, *leu2*Δ0, *ura3*Δ0, p*MET15*)	This study	N/A
Oligonucleotides		
See Table S1 for list of primers	This study	N/A
Recombinant DNA		
Plasmid p*HIS3*	Mülleder et al.[87]	Addgene #64178
Plasmid p*LEU2*	Mülleder et al.[87]	Addgene #64177
Plasmid p*URA3*	Mülleder et al.[87]	Addgene #64180
Plasmid p*MET15*	Mülleder et al.[87]	Addgene #64179
Software and algorithms		
Pyphe	Kamrad et al.[92]	https://github.com/Bahler-Lab/pyphe
DeadOrAlive	Romila et al.[91]	https://github.com/JohnTownsend92/DeadOrAlive
BD Diva software, version 8.0.1	BD Biosciences	https://www.bdbiosciences.com/en-de/products/software/instrument-software/bd-facsdiva-software
FlowJo software, version 10.3.0.	BD Biosciences	https://www.flowjo.com/solutions/flowjo
DIA-NN	Demichev et al.[58]	https://github.com/vdemichev/DiaNN
iPath3	Darzi et al.[60]	https://pathways.embl.de/
Agilent MassHunter Quantitative Analysis 10.1	Agilent	https://www.agilent.com/en/product/software-informatics/mass-spectrometry-software/data-analysis/quantitative-analysis
LabSolutions Lite for LC-PDA software	Shimadzu	https://www.shimadzu.de/labsolutions%E2%84%A2-lcms-software-simple-analytical-platform

RESOURCE AVAILABILITY

Lead contact

Further information and requests for resources and reagents should be directed to and will be fulfilled by the lead contact, Markus Ralser (markus.ralser@charite.de).

Materials availability

This study did not generate new unique reagents.

Data and code availability

- The data supporting the findings of this study are available within the paper, its supplemental information and is deposited within publicly accessible repositories. The mass spectrometry proteomics data of chronologically aging SeMeCo, relevant to data shown in Figures 4, 6, S5, and S6, have been deposited to the ProteomeXchange Consortium via the PRIDE[86] partner repository with the dataset identifier PRIDE: PXD036444. The mass spectrometry proteomics data of wild-type yeast supplemented with/out amino acids, relevant to data shown in Figure S3C, have been deposited to the Mendeley repository with dataset identifier Mendeley Data: https://doi.org/10.17632/sd8zthmrk4.1.
- Yeast gene functions and GO slim term mapper can be accessed at the Saccharomyces Genome Database (SGD: https://www.yeastgenome.org/). Protein sequence databases used for the identification and mapping of proteins from proteomics can be accessed via Uniprot:https://www.uniprot.org/ and KEGG: https://www.genome.jp/kegg/pathway.html. No custom software codes were generated as part of this study. All analyses conducted in R v4.1.3. used standard, publicly accessible packages obtained either through GitHub (https://github.com/), the Comprehensive R Archive Network (CRAN, https://cran.r-project.org/) or via Bioconductor (https://www.bioconductor.org/).
- Any additional information required to reanalyse the data reported in this paper is available from the lead contact upon request.

EXPERIMENTAL MODEL AND SUBJECT DETAILS

Yeast strain construction

The haploid BY4741 *S. cerevisiae* strain (MATa: *his3*Δ1, *leu2*Δ0, *ura3*Δ0, *met15*Δ0) was used to generate all subsequent strains used in the study (key resources table). Prototrophy was restored with the wild-type locus of *HIS3*, *LEU2*, *URA3* and *MET15* either by genomic integration (knock-in), with primer design based on information from Brachmann et al.[29] or plasmid complementation generated by Mülleder et al.[87] (see key resources table), followed by standard cloning and yeast transformation techniques.[88] Primers were designed to flank the genomic region of the gene of interest ± several hundred base pairs to maximise the homologous region for recombination. The YSBN5 yeast strain was used as template DNA. Primer sequences for genomic integration of the metabolic markers as follow: *HIS3* Fw: 5'TATCGTTTGAACACGGCATT3' and Rv: 5'CGCG CCTCGTTCAGAATGAC3'; *LEU2* Fw: 5'GAATTAAAGGATTGGATAGC3' and Rv:5'CCCTATGAACATATTCCATT3'; *URA3* Fw: 5'GTTCATCATCTCATGGATCT3' and Rv: 5'TACTGTTACTTGGTTCTGGC 3'; *MET15* Fw: 5'TCGTTTTCTACTTTCTTCTG3' and Rv: 5'GGAGAAGTCAAGACTATGAA3'.

All strains are long-term stored in −80°C using a glycerol-based standard storage medium (glycerol 30% v v^{-1}).

METHOD DETAILS

Yeast strains culture

SeMeCo strain generation and culture

The generation and culture of SeMeCo was performed as previously described.[22] The p*HIS3*, p*LEU2*, p*URA3* and p*MET15* plasmids were used to generate a SeMeCo strain in the BY4741 background.[87] All SeMeCo strains were cultured in minimal synthetic (SM) media, composed of yeast nitrogen base without amino acids (YNB, 6.8 g/L) + 2% glucose (20 g/L), so cells rely on the exchange of self-synthesised metabolites for growth and survival. Briefly, cryo stocks were streaked onto SM + 2% agar medium and cultured at 30°C for 3 days. Then, a micro-colony was diluted in 500 μL dH_2O, and normalised to OD_{600nm} = 0.8. Then, 5 μL were spotted onto a solid SM medium to generate a giant colony. This initial spotting corresponded to ~7.2 × 10^4 cells using a predefined OD-to-cell number standard curve. Cells were incubated for 2 days at 30°C, then giant colony generation was repeated to ensure cells have undergone enough proliferation cycles and plasmid segregation, enabling metabolic cooperation, whilst being continuously kept in an exponential growth phase. Pre-cultures were generated by diluting the giant spots into 1 mL dH_2O, normalised to OD_{600nm} = 1 in SM liquid medium and cultured for 16 hours at 30°C. Cultures were then generated by diluting the pre-cultures to OD_{600nm} = 0.1 in SM liquid medium and cultured for the duration of the CLS. This relatively high starting OD_{600nm} ensures cells are kept at a density that minimises disturbing the relative proportions of auxotrophs and prototrophs generated in the SeMeCo. Cells were collected for downstream experiments at different growth phases, as indicated in figure legends. The control wild-type strain (BY4741, quadruple knock-in: *HIS3*, *LEU2, URA3* and *MET15*), herein referred to as the prototrophic wild-type strain, followed the exact same procedures as SeMeCo. Strain details are in the key resources table.

For CLS assays cells were grown either on glucose (SM supplemented with 2% glucose) or glycerol (SM supplemented with 3% glycerol and 0.1% glucose). SeMeCo generation and respective wild-type controls were grown on solid SM supplemented with glucose prior to being cultured in SM supplemented with glycerol from pre-culture stage onwards.

Knockout strain culture

Knockout strain cultures followed the exact same culture procedure as described for SeMeCo generation and culture. In the case of the *met15Δ* strain, cells were grown on SM media supplemented with 20 mg/L L-methionine, with respective wild-type controls also being cultured in SM supplemented with methionine.

Exometabolome exchange cultures

Prototrophic wild-type and SeMeCo yeast cells were cultured in parallel, in SM media supplemented with 2% glucose, for 48 hours (until the stationary phase). Culture media was then collected by spinning down cells in each culture at 3,000 *g* for 5 min at room temperature (RT), followed by supernatant (media) filtering with a 0.22-μm syringe filter. Experimental wild-type culture cell pellets were then gently resuspended in the filtered media (exometabolome) from SeMeCo, whilst control wild-type cell pellets were resuspended back in their own filtered culture media. Wild-type cultures either in SeMeCo or wild-type exometabolomes were then followed for CLS.

Cultures for isotope labelling

For assessing amino acid import during chronological lifespan, prototrophic wild-type yeast cells were cultured in 10 mL SM media supplemented with 2% of either ^{12}C-glucose or ^{13}C-glucose for 48 hours. The media was then swapped as follows: the full volume of culture media was collected by spinning down cells in each culture at 3,000 *g* for 5 min at room temperature (RT), followed by supernatant (media) filtering with a 0.22-μm syringe filter. Filtered supernatants were then added to respective swap cultures and cells were gently resuspended. Then 650 μL of each sample were collected for isotope tracing amino acid analysis using targeted metabolomics by HPLC-MS/MS,[38] at 2, 6, 24, 48 and 72 hours post media swap (plus a control 0 hours collection, just prior swapping media). Control cultures were swapped from SM supplemented with ^{13}C-glucose to SM supplemented with ^{12}C-amino acids (Yeast Synthetic Drop-out Medium Supplements, without lysine; Sigma, Cat# Y1896, final concentration of 3.1 g/L). Absence of lysine in the amino acid supplementation mix was an additional control, whereby cells swapped to the mixture should not present imported ^{12}C-lysine.

For analysing the switch from synthesis to uptake upon methionine supplementation by ^{13}C isotope tracing metabolomics, the prototrophic wild-type strain was grown to mid-log phase in 96 deep-well plates with 200 μL SM media with 1% ^{13}C glucose and varying methionine concentrations.

In both cases, cells were harvested by centrifugation (4 min, 3,200 *g*), washed in water and metabolites were extracted as described below for *"intracellular and extracellular amino acid and uracil quantification"*.

Amino acid supplemented cultures for proteomics

For analysing the impact of amino acid supplementation on the proteome, the prototrophic wild-type strain was cultured in 1.4 mL SM media in 96 deep well plates with a starting OD_{600nm} of 0.05 with and without a synthetic supplement mix (Sigma, Cat# Y1896, final concentration of 3.1 g/L). After 10 hours, cell pellets were harvested by centrifugation (4 min, 3,200 *g*) and proteomes were analysed as described below.

Growth assays

Growth was assessed by monitoring biomass formation using optical density absorbance at a wavelength of 600 nm (OD_{600nm}). OD_{600nm} was recorded either manually during the CLS, on an Ultrospec 2100 Pro™ spectrophotometer (Amersham Biosciences), or automatically on a plate reader (NanoQuant Plate™, Infinitive 200 PRO (Tecan)) every 10 minutes, until cells reached stationary phase, at 30°C for growth-curve recording. Both maximum growth and time to mid-log phase were determined from growth curves data using the R 'growthcurver' package.[89]

Chronologic lifespan

Conventional and high-throughput colony forming unit (CFU) assays

Conventional CFU analysis was performed as described previously[90] by aliquoting equal volumes of aging cultures throughout CLS and plating cells at different dilution factors into solid rich media (YPD) composed of yeast extract (10 g/L), peptone (20 g/L), dextrose/glucose (20 g/L) and agar (20 g/L). Cells were incubated for 2 days at 30°C and the number of CFUs was recorded. Increasing numbers of cultures analysed in parallel required the usage of a high-throughput CFU (HTP-CFU) method as described in Romila et al.[91] Briefly, 200-μL aliquots of aging culture were loaded into the first column of a 96-well plate (8 cultures in parallel per plate). The rest of the plate was loaded with 100 μL of dH_2O. Using a Biomek NX^P automatic liquid handler (Beckman Coulter), 50 μL of the aging culture from the first column were serially diluted 3-fold across the plate, ensuring each dilution factor was well mixed. Droplets of serially diluted aging cultures were immediately dispensed onto solid YPD in quadruplicate (384-well format) using a Singer RoToR HDA pinning robot (Singer Instruments). For this, long-pin 96-density pads were used, making sure that the source plate was revisited before each pin onto the agar. Plates were incubated for 2 days at 30°C until patterns of colonies appeared. Images of agar plates were acquired with Pyphe-scan[92] using an Epson V700 scanner in transmission mode. Plate image analysis and quantification of the number of CFUs in the aging culture, based on the colony patterns observed, were performed using the R package 'DeadOrAlive'.[91] In both conventional- and HTP-CFU assays, survival of the different strains was normalised, first to dilution factor, then to biomass measured at the time of sample collection, as measured by OD_{600nm}, and then to the survival of the respective wild-type controls at the beginning of the stationary phase (48 hours from the start of culture).

Maximum lifespan

Maximum lifespans were calculated from CFU colonies at the latest time point where at least 96 colonies formed per biological replicate (for at least 3 biological replicates per strain), from 100 μL of undiluted stationary culture spread on agar, for accurate metabotyping analysis.

Live/Dead staining

Cell death was assessed using the LIVE/DEAD™ Fixable Far Red Dead Cell Stain Kit, for 633 or 635 nm excitation (Invitrogen™, ThermoFisher Scientific) according to the manufacturer's instructions, followed by high-throughput flow cytometry (HTP-FC). Briefly, an aliquot of 300 μL of each aging culture was transferred to a 96-deep-well plate. Plates were then spun down at 3,000 *g* for 3 min RT, the supernatant was discarded, and cells were resuspended in 300 μL of diluted dye (1:1000 diluted stock dye in dH_2O), followed by an incubation of 30 min in the dark. Cells were then washed in 500 μL of dH_2O, resuspended in 300 μL of ~4% formaldehyde (37% formaldehyde diluted 1:10 in PBS 1x) and incubated 10 min in the dark. Cells were washed in PBS 1x and stored in 500 μL fresh PBS 1x at 4°C, protected from light, until analysis by HTP-FC. Immediately prior to analysis, samples were sonicated for 20 s at 50W (JSP Ultrasonic Cleaner US21) to maximize cell singlets for HTP-FC analysis, and 250 μL were transferred to a 96-well plate for HPT-FC analysis. For HTP-FC, 30,000 cells/sample were measured in a Fortessa X20 flow cytometer (BD Biosciences), using the HTS plate mode on the BD Diva software version 8.0.1. and a 633-nm excitation laser to capture the dye staining. Populations of interest were gated using the FlowJo software version 10.3.0. Features of interest (dead and live cell populations) were then exported for further analysis using R.

Metabotyping

Metabotyping was performed as previously described,[39] with the difference that colonies were cryostocked prior to replica-plating, so cells collected at different time points across the CLS would be analysed in parallel. Firstly, conventional CFUs were performed as described above. Then 96 individual CFUs per biological replicate were resuspended in 100 μL of liquid YPD supplemented with 30% glycerol in a 96-well plate (Nunc™ Sigma), as one colony/well, then incubated at 30°C ON prior to freezing at –80°C. Once all samples across the CLS were collected, plates were defrosted and then replica-plated on six plates, containing either (a) complete medium (SM with all four missing nutrients: 20 mg/L of L-histidine, L-uracil and L-methionine and 60 mg/L of L-leucine), (b) SM medium, and plates with SM and all nutritional supplements except (c) L-histidine, (d) L-leucine, (e) L-uracil or (f) L-methionine. The absence of growth in a particular drop-out medium reflects the clone auxotrophy for that specific metabolite. The combinatorial growth ability in the six different media allows determination of each clone metabotype (total auxotrophies it contains). This method permits identification of all 16 possible metabotypes resulting from all possible combinations of the four auxotrophies. Segregants abundance was relative to all metabotypes, including non-segregant prototrophic cells, in SeMeCo, as follow: % auxotrophs = (n auxotrophs/ (n auxotrophs + n prototrophs)*100). Statistics were calculated by pairwise comparing relative abundance of each segregant to their relative abundance in the early stationary phase (day 2), by paired two-sided t test.

pH analysis

Aliquots of 1 mL were collected per culture at different time points during the CLS and pH was measured using a Mettler-Toledo InLab® Micro & Micro Pro pH electrode coupled to pH/Ion bench meter SC S220-B (Mettler Toledo).

Oxygen consumption

10 mL of CLS cultures were collected during exponential (day 1) and early stationary phase (day 2), placed into a 10-mL Erlenmeyer flask and stirred at 900 rpm using a magnetic stirrer bar. An oxygen probe (Hanna HI 98193) was inserted into the flask in such a way that it became completely filled with no remaining air inside it. The flask was sealed with parafilm to impede gas exchange. The oxygen saturation of the culture was recorded twice: 0 and 5 min. Oxygen levels were normalised to biomass and live cells, as measured by OD_{600nm} and CFU analysis respectively, and to levels of wild-type at the beginning of measurements (0 min).

Reactive Oxygen Species Levels

Hydrogen peroxide levels, as a readout of intracellular ROS levels, was assessed using the Dihydrorhodamine 123 (DHR, Invitrogen™, ThermoFisher Scientific) according to the manufacturer's instructions, followed by high-throughput flow cytometry (HTP-FC). Briefly, an aliquot of 300 μL of each ageing culture was transferred to a 96-deep-well plate. DHR was added to each well to a final concentration of 10 μM and incubated at 30°C for 15 min in the dark. Cells were then spun down at 3,000 *g* for 3 min RT and the supernatant was discarded. Cells were then subject to 3 cycles of washes in 500 μL of dH_2O, spinning down at 3,000 *g* for 3 min RT and discarded supernatant. Cells were resuspended in 500 μL of PBS 1x before being sonicated for 20 s at 50W (JSP Ultrasonic Cleaner US21) to maximise cell singlets for HTP-FC analysis. 250 μL were transferred to a 96-well plate for HPT-FC analysis. For HTP-FC, 30,000 cells/sample were measured in a Fortessa X20 flow cytometer (BD Biosciences), using the HTS plate mode on the BD Diva software version 8.0.1. and a 488-nm excitation laser to capture the dye staining. Populations of interest were gated using the FlowJo software version 10.3.0. Features of interest (DHR intensity) were then exported for further analysis using R.

Targeted metabolomics

Intracellular glycolytic and TCA intermediates, nucleotides and amino acids

Sample Preparation. Aging cultures, at several time points reflecting different growth phases, were sampled and 400 μL of each culture were quenched in 1,600 μL dry-ice-cold LC-MS grade methanol (MeOH), into a 48-deep-well plate, as described by Ewald et al.[93] This suspension was spun down (600 g, 3 min, 4°C), and the supernatant was discarded by inversion, followed by a short spin (600 g, 1 min, 4°C) to ensure complete removal of the SN. Cell pellets were immediately placed on dry ice and then transferred to −80°C until analysis. As an internal control, metabolites from ^{13}C labelled *Synechococcus sp.* were extracted, and MeOH concentration adjusted to 71.4% (corresponding to 10:4 MeOH/water) and immediately stored at -20°C to avoid degradation. Intracellular metabolites from samples were then extracted as described.[94] Briefly, 140 μL of extracted ^{13}C labelled *Synechococcus sp.* metabolites (in 10:4 MeOH/water) were added and vortexed. Then, 50 μL chloroform was added, followed by 50 μL water and 50 μL chloroform with thorough mixing in between. Phases were separated by centrifugation at 3,000 g for 5 min. The aqueous phase was recovered and used without further conditioning. Standards was stepwise diluted and each mixed with the same amount of ^{13}C labelled *Synechococcus sp.* metabolites. The order of samples was randomised and one microliter was injected for HPLC–MS/MS analysis.

Sample Acquisition. Metabolites were resolved on an Agilent 1290 Infinity II high-performance liquid chromatography (HPLC) system by hydrophilic interaction liquid chromatography (HILIC) coupled to an Agilent 6470 triple quadrupole instrument operating in dynamic MRM (dMRM) mode, as previously described.[31] In short, the gradient program started at 30% solvent B (100 mM ammonium bicarbonate) and was kept constant for 3 min before a steady increase to 60% solvent B over 4 min. Solvent B was maintained at 60% for 1 min before returning to initial conditions. The column was washed and equilibrated for 2 min, resulting in a total analysis time of 10 min. We used acetonitrile as solvent A and a Waters BEH Amide column (2.1 × 100 mm, 1.7 μm particle size) for separation. The flow rate was set to 0.3 mL/min and column temperature to 35°C. Compounds were identified by comparing retention time and fragmentation patterns with analytical standards. Quantification of metabolites that were below the limit of detection was excluded from analysis. Metabolite quantifications were then normalised per biomass, as measured by OD_{600nm}, at the time of collection.

Intracellular and extracellular amino acid and uracil quantification

Sample Preparation. Aging cultures, at several time points reflecting different growth phases, were sampled and 500 μL of each culture were collected into a 96-deep well plate for amino acid and uracil profiling. Samples were centrifuged at 4,000 *g* for 3 min and supernatants (SN) were transferred into a new 96-deep well plate for extracellular metabolite profiling, whilst cell pellets were washed once in 500 μL of dH_2O, spun down at 4,000 *g* for 3 min and SN was discarded (followed by a 1 min spin for complete removal of SN) for later intracellular metabolite profiling. Both cell pellets and SN were immediately frozen in dry ice and samples were then stored at −80°C until analysis.

The amino acid and uracil extraction, separation and detection protocols were adapted from Mülleder et al.[38] Briefly, 200 μL of 80% LC-MS grade ethanol at 80°C were added to the yeast pellets. Samples were heated for 2 min at 80°C, vigorously mixed on a vortex mixer and incubated for further 2 min at 80°C followed by vigorous vortexing. The extracts were removed from debris by centrifugation at 12,000 *g* for 5 min. SN were also centrifuged at 12,000 *g* for 5 min to further purify samples from any debris.

For analysing of the switch from synthesis to uptake upon methionine supplementation by ^{13}C metabolomics, following the ethanol extraction, samples were dried in a Speedvac at 30°C and reconstituted in 10 μL of 1:2 methanol:water with 10 mM ammonium formate and 0.176% formic acid, followed by the addition of 65 μL acetonitrile (to match the starting conditions of the LC-MS/MS method). The order of samples was randomised, and one microliter was injected for HPLC–MS/MS analysis.

Sample Acquisition. For analysis by HPLC–MS/MS, amino acids and uracil were separated by HILIC using an ACQUITY UPLC BEH amide column (130 Å, 1.7 mm, 2.1 mm × 100 mm) on a liquid chromatography (Agilent 1290 Infinity II HPLC) and tandem mass spectrometry (Agilent 6460) system. Buffer A was composed of 50:50 acetonitrile/water, 10 mM ammonium formate and 0.176% formic acid, and buffer B of 95:5:5 acetonitrile/methanol/water, 10 mM ammonium formate, and 0.176% formic acid. The gradient elution was performed at a constant flow rate of 0.9 mL/min. Starting conditions were 85% buffer B, after 0.7 min the concentration of buffer B was decreased gradually to 5% until 2.55 min and kept for a further 0.05 min before returning to initial conditions. The column was then equilibrated, resulting in a total runtime of 3.25 min. Compounds were identified by matching retention time and fragmentation (MS2) with commercially obtained amino acid and uracil standards (see key resources table). Signals for free amino acids and uracil were then acquired in dynamic SRM mode in the MassHunter Software as previously described.[38] Compounds were identified by comparing retention time and fragmentation patterns with analytical standards. Amino acid and uracil quantifications were then normalised per biomass, as measured by OD_{600nm}, at the time of collection.

Extracellular amino acids and uracil data from wild-type in exponential phase are a re-analysis of data in[22]; experiments, whereby cell culture, metabolite extraction and sample acquisition, were followed for CLS analysis.

For LC-MS analysis for the isotope tracing experiments (Figures 1E and S3B), we extended the gradient elution at a flow rate of 0.6 ml/min, as follows: isocratic separation for 3 min with 85% solvent B, decrease to 5% B over 7 min, 1 min wash before returning to starting conditions with 2 min equilibration. The monoisotopic ^{12}C and fully ^{13}C-labelled metabolites were monitored.

Intracellular polyamines

Sample Preparation. Cell pellets from aging cultures were collected and processed as described above for "intracellular and extracellular amino acids and uracil", where intracellular metabolites from −80°C stored cell pellets were ethanol extracted. The spun dried pellet obtained, after evaporation of ethanol in a vacuum concentrator (Thermo Scientific SPD300DDA, 30 °C, 200 mTorr,

2h), was resuspended in HPLC grade water containing an external standard, which from here on is denoted as SN. The SN was then derivatised for polyamines prior HPLC–MS/MS analysis using a protocol adapted from Wong et al.[95] Briefly, 10 μL of SN were transferred into a 500 μL deep-well plate. To this were added sequentially 2 μL pyridine (1 M in acetonitrile), 10 μL of 100 mM aqueous sodium carbonate and 20 μL of 2% benzoyl chloride in acetonitrile (freshly prepared). Following a brief mixing (5 s) and incubation (1 min, 25°C), the plate was centrifuged (3,000 g) to settle any precipitate. The supernatant was transferred to a fresh plate for HPLC–MS/MS analysis. An external calibration standard mixture was prepared in MQ water in a serial dilution of 1:5:5:5:5:5 and derivatised as above. Fresh media (SM) was used as a blank for derivatisation.

Sample Acquisition. HPLC–MS/MS measurement was carried out on an Agilent 1290 Infinity II HPLC coupled to an Agilent 6495 triple quadrupole mass spectrometer. The HPLC parameters were as follows: Solvent A and B were respectively 0.1% formic acid in water and 0.1% formic acid in acetonitrile. The chromatography was carried out using Agilent ZORBAX Eclipse Plus Phenyl-Hexyl column (2.1 × 100 mm) maintained at 30°C and a flow rate of 0.3 mL/min. The applied solvent composition consisted of 50% solvent B from 0 to 3.9 min followed by 100% solvent B from 4 to 6 min. The column was then re-equilibrated at 50% solvent B from 6.1 to 7.5 min. The MS parameters were as follows: gas flow at 11 L/min and 230°C, sheath gas flow at 10 L/min and 350°C, nebuliser pressure at 35 psi, fragmentor voltage at 166 V, capillary voltage at 2500 V (positive) and nozzle voltage at 1000 V. Cell acceleration voltage was set at 7 V. A volume of 2 μL was injected and the analysis was carried out as dMRM in the positive mode. Transitions monitored for dMRM were used as follow for: putrescine: transition (T)= 297.2->105 & 176.2, retention time (RT) = 1.066±0.5 min and collision energy = 20 & 12 V; Spermidine: T= 483.3->105 & 336.4, RT= 1.34±0.5 and CE = 60 & 16; Spermine: T= 619.3->105 & 497.3, RT= 1.697±0.5 and CE= 76 & 24. The generated data was processed using Agilent MassHunter Quantitative Analysis 10.1 software. Measurements below the limit of quantification were excluded from further analyses. Polyamines quantifications were then normalised per biomass, as measured by OD_{600nm}, at the time of collection.

HPLC method for ethanol, acetate and glycerol exometabolome quantification

Sample Preparation. Frozen supernatants in 96-deep well plates collected as described above for "intracellular and extracellular amino acids and uracil" were defrosted and kept shaking using a plate shaker for 20 min at 900 rpm at room temperature just before the filtration step. Supernatants were filtered using a multiscreen filtered plate with 0.45 μm durapore membrane (MVHVN4525), a Strata well plate manifold (https://phenomenex.blob.core.windows.net/documents/863d86a0-3aba-4591-979b-bf54b1188038.pdf) and a Welch vacuum pump.

Sample Acquisition. Target compounds were quantified using a Shimadzu Prominence HPLC (https://www.ssi.shimadzu.com/products/liquid-chromatography/prominence-hplc.html) equipped with a refractive index detector RID20A and a Sil20-ACT auto sampler with a 96-well plate injector tray. Chromatographic separation was performed on an Agilent Hi-plex H column (https://www.agilent.com/cs/library/applications/5990-8801EN%20Hi-Plex%20Compendium.pdf). The temperature of the column and detector was 50°C and 41°C, respectively. The eluent was 0.00125 N H_2SO_4 in ultrapure water (0.6 mL min^{-1}). The samples were kept in 96-well plates (https://www.sarstedt.com/en/products/laboratory/cell-tissue-culture/cultivation/product/83.3926/) covered with a silicone mat (https://www.phenomenex.com/Products/Part/AH0-8633) at 4°C in the autosampler prior the injection for no longer than 2 days. 5 μL was injected from the samples/well plates as well as standard compounds. The method works with a 26-min cycle time. To keep the retention times and detector response constant, 5 L of eluent was mixed in a single batch.

Data were analysed using the Shimadzu LabSolutions Lite for LC-PDA software. Target compounds were identified using automated retention time matching with individual standards of an in-house overflow metabolite library dissolved in SM minimal media. Compound concentrations were calculated using peak area integration with pre-optimised integration parameters and external calibration for each compound. All calibration curves showed high linearity (R^2 > 0.998) over a 3-order-of-magnitude concentration range. Integration and compound identification were manually overviewed. Data were then exported and further processed using R. Metabolite quantifications were normalised per biomass, as assessed by OD_{600nm} , at the time of collection.

Data Independent Acquisition (DIA)- based proteome profiling

Sample Preparation. Aging cultures, at several time points reflecting different growth phases, were sampled and 500 μL of each culture were collected into a 96-deep well plate. Samples were centrifuged at 4,000 *g* for 3 min and supernatants (SN) were discarded. Samples were centrifuged again at 4,000 *g* for 1 min to fully remove any residual SN. Cell pellets were immediately placed on dry ice before being stored at –80°C until all samples were collected. Sample preparation for proteomics was performed as previously described.[96] Briefly, cell pellets were processed in a bead beater for 5 min at 1,500 rpm (Spex Geno/Grinder) in a lysis buffer where proteins were denatured in 8 M urea plus 0.1 M ammonium bicarbonate at pH 8.0. Samples were spun down for 1 min at 4,000 g before they were reduced in 5 mM dithiothreitol for 1 h at 30°C, then alkylated in 10 mM iodoacetamide for 30 min at RT protected from light. Samples were diluted to less than 1.5 M urea in 0.1 M ammonium bicarbonate at pH 8.0, before proteins were digested overnight at 37°C with trypsin. Trypsin was neutralised with 1% formic acid (FA) before peptides were cleaned-up in 96-well MacroSpin plates (Nest Group): 1. plates were first equilibrated in a series of methanol (1x), 50% acetonitrile (ACN, 2x), and 3% ACN 0.1% FA (2x); between each wash plates were spun down for 1 min at 100 *g* and the flow-through was discarded; 2. samples were loaded into the plates and peptides were cleaned up in a series of 3% ACN, 0.1% FA (3x); between each wash samples were spun down for 1 min at 100 *g* and flow through was discarded; 3. peptides were eluted into a new collection plate with 50% ACN (3x) and spun-dried overnight at RT in a speed vacuum. Peptides were then dissolved in 40 μL of 3% ACN 0.1% FA. Peptide concentration was measured at 280 nm using a Lunatic spectrometer system (Unchained Labs).

Sample Acquisition. The digested peptides were analysed on a nanoAcquity (Waters) (running at 5 μL min^{-1} microflow liquid chromatography) coupled to a TripleTOF 6600 (SCIEX). Protein digest (2 μg) was injected and the peptides were separated with a 23 min non-linear gradient starting with 4% ACN in 0.1 % FA and increasing to 36% ACN in 0.1% FA. A Waters HSS T3 column (150 mm × 300 μm, 1.8 μm particles) was used. The Data Independent Acquisition (DIA) method consisted of an MS1 scan from m/z 400 to m/z 1250 (50 ms accumulation time) and 40 MS2 scans (35 ms accumulation time) with a variable precursor isolation width covering a mass range from m/z 400 to m/z 1250. Data quantification was performed using DIA-NN version 1.7.10 software.[58] Post-processing data analysis was conducted in R.[97]

Genome-scale metabolic modelling (flux balance analysis)

The community metabolic models were reconstructed using the approach from our previous study.[22] Briefly, the list of auxotrophic marker genes for amino acids and nucleobase (U) was obtained from the Saccharomyces Genome Database (SGD[98]). The genome-scale metabolic model of *S. cerevisiae*[99,100] was used to create auxotrophic strain models by switching off respective metabolic reactions for each metabolic gene. The growth of the auxotroph model was optimised by supplementing respective metabolites together with the minimal media components and if the model was able to produce biomass, then the auxotrophic strain was considered for creating a community model. The reactions from auxotroph (different amino acids and/or nucleobase H, L, M and/or U) and prototroph (WT) models were combined to make the community, using the compartment per guild approach, where both strains were treated as separate compartments and metabolic exchange between strains was allowed. The community biomass was the combined biomass of all strains. The Cobra toolbox[101] was used to perform the model simulations. Only genes in which an auxotrophy can be introduced by a single-locus deletion were modelled (some amino acid auxotrophs would require multiple-locus deletion).

QUANTIFICATION AND STATISTICAL ANALYSIS

Post-processing data analysis and statistical analyses were done in R v4.1.3 (R Core Team, www.R-project.org) using specific packages as indicated throughout the STAR Methods section. The CRAN R packages: 'tidyverse' was used for basic data manipulation and visualisation and the 'ggpubr' package for statistical analysis. Hypothesis testing to assess means of population differences was mainly done using ttest, whenever the variables could be assumed continuous, or otherwise using Wilcoxon rank-sum test, as indicated in the respective figure legends. Sample-size estimations were not performed in any of the experiments. All experiments were performed using at least n = 3 biological replicates. Missing values in the proteomics data were median imputed. The Gene Ontology (GO) slim term mapper from the SGD database[98] was used to map differentially expressed proteins with GO slim terms. The KEGG term mapper from the KEGG database[102] was used to map differentially expressed proteins with KEGG terms. For the proteome analysis of the aging SeMeCo (Figure 4A), GO slim and KEGG enrichment analysis of differentially expressed proteins was performed using the 'ClusterProfiler' R package. For the proteome analysis of the wild-type yeast supplemented with amino acids (Figure S3C), analysis was performed using the 'Limma' R package.[103] Metabolic enzyme expression levels were mapped to the yeast metabolic network using iPath3.[60]

CellPress
OPEN ACCESS

Supplemental figures

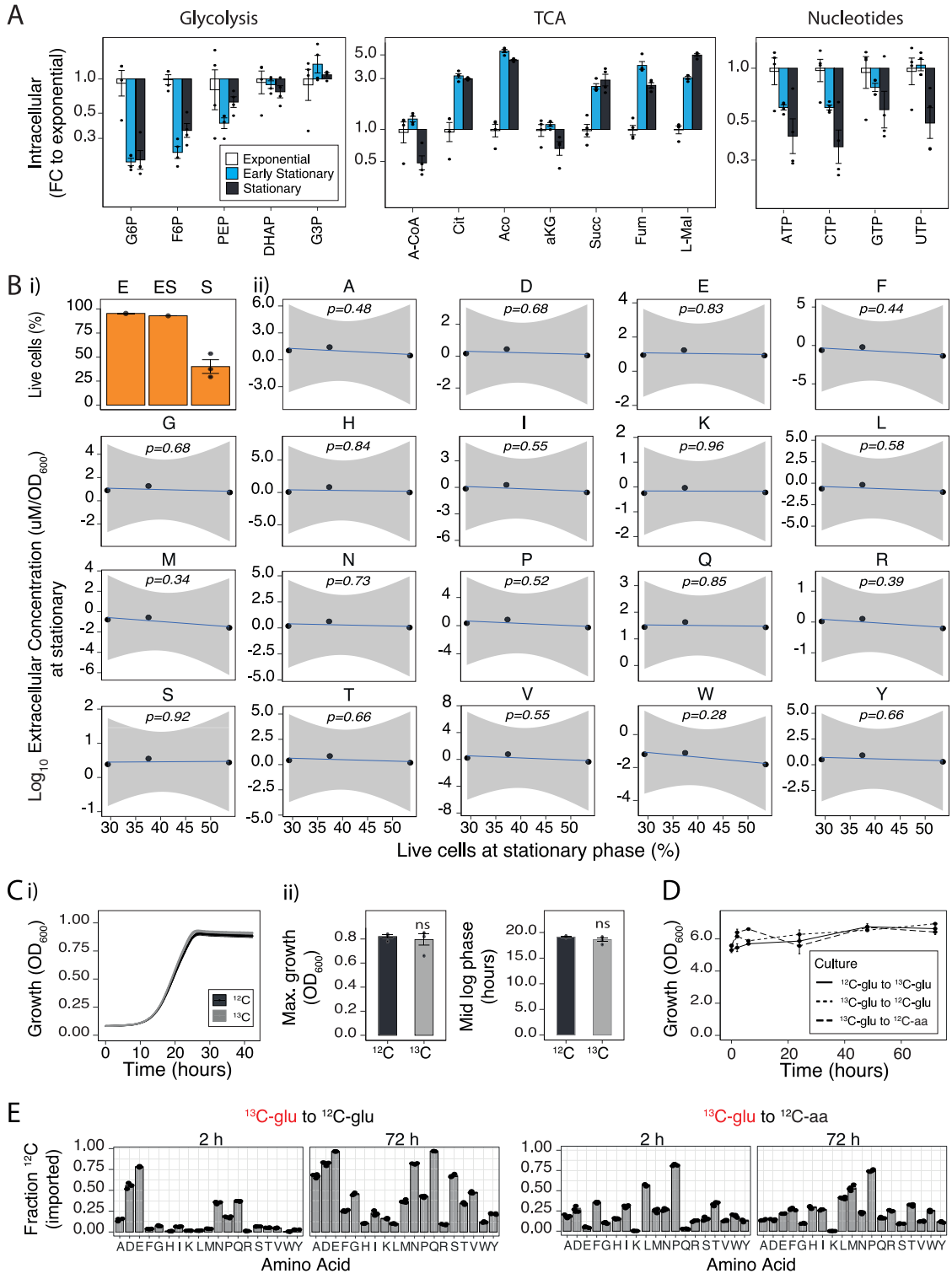

(legend on next page)

Figure S1. Yeast cells establish cross-generational metabolite exchange interactions, related to Figure 1

(A) Quantification of intracellular metabolites levels by targeted metabolomics[31] (see STAR Methods), categorized by metabolic pathway, during CLS as described in Figure 1A. Bar plots show mean ± SEM fold change (FC) to levels in the exponential phase of n = 4 biological replicates; dots represent independent cultures. G6P, glucose-6-phosphate; F6P, fructose-6-phosphate; PEP, phosphoenolpyruvic acid; DHAP, dihydroxyacetone phosphate; G3P, glyceraldehyde-3-phosphate; A-CoA, acetyl coenzyme A; Cit, citrate; Aco, aconitate; aKG, alpha-ketoglutarate; Succ, succinate; Fum, fumarate; L-Mal, L-malate; ATP, adenosine triphosphate; CTP, cytidine triphosphate; GTP, guanosine triphosphate; UTP, uridine triphosphate. Statistics by unpaired two-sided Wilcoxon rank-sum test and multiple testing correction using the BH method; adjusted p values in Table S1.

(B) (i) Cell viability analysis, using the LIVE/DEAD fixable dye (see STAR Methods), of aging wild-type yeast cultures, as described in Figure 1A. Bars plots show the percentage of live cells in the different growth phases. Data are mean ± SEM of n = 3 biological replicates (dots represent independent cultures values). (ii) Pearson correlation between extracellular amino acid levels (from Figure 1C) and the percentage of live cells in stationary phase cultures (from i). Data are from n = 3 biological replicates (dots represent individual cultures); error bands indicate the 95% confidence level interval for the predictions from the linear model.

(C) Wild-type yeast cells cultured in SM media supplemented either with ^{12}C-glucose (^{12}C-glu) or ^{13}C-glucose (^{13}C-glu), then media was swapped for tracing amino acid import, using targeted metabolomics[38] (see STAR Methods), as described in Figure 1Ei). Control cultures were swapped from SM supplemented with ^{13}C-gluc to SM supplemented with ^{12}C-amino acids (^{12}C-aa), without glucose, at standard culturing concentrations. Prior media swap (i) growth curves and (ii) maximum growth and time to mid-log phase, as measured by $OD_{600nm,}$ of wild-type yeast cells grown on SM media supplemented either with 2% ^{12}C-glu or ^{13}C-glu. Data mean ± SEM of n= 4 biological replicates/per condition (culture media). Statistics by unpaired two-sided Wilcoxon rank-sum test; p value = ns (>0.05, not statistically significant); maximum growth p value = 0.883; time to mid-log phase p value = 0.686.

(D) Biomass, as assessed by OD_{600nm}, measured at 0, 2, 6, 24, 48, and 72 h, post media swap from SM + ^{13}C-glu to ^{12}C-glu (^{13}C-glu to ^{12}C-glu), or SM + ^{12}C-amino acids (^{13}C-glu to ^{12}C-aa), or from SM + ^{12}C-gluto SM + ^{13}C-glu (^{12}C-glu to ^{13}C-glu). Data mean ± SEM of n = 4 biological replicates/per condition (culture media swap). Statistics by unpaired two-sided Wilcoxon rank-sum test; p values in Table S2.

(E) Fraction of intracellular ^{12}C-aa in ^{13}C-glu to ^{12}C-glu and ^{13}C-glu to ^{12}C-aa cultures at 2 and 72 h post media swap, showing the uptake of extracellular ^{12}C-aa as indicated by the gradual increase in the intracellular fraction of ^{12}C-aa in both cultures. Total aa levels, measured as area under the curve (AUC), were normalized per biomass, assessed by OD_{600nm}. Bar graphs represent the mean fraction of intracellular ^{12}C labeled aa fractions of n = 4 biological replicates/per condition (culture media swap); dots represent independent cultures fractions. Statistics by unpaired two-sided Wilcoxon rank-sum test; p values are listed in Table S2.

Note: the amino acid mix supplemented does not contain lysine; as an extra control, we observe all amino acids present in the mixture were imported (as shown by the ^{12}C labeling) except lysine (^{12}C), which we do not detect intracellularly.

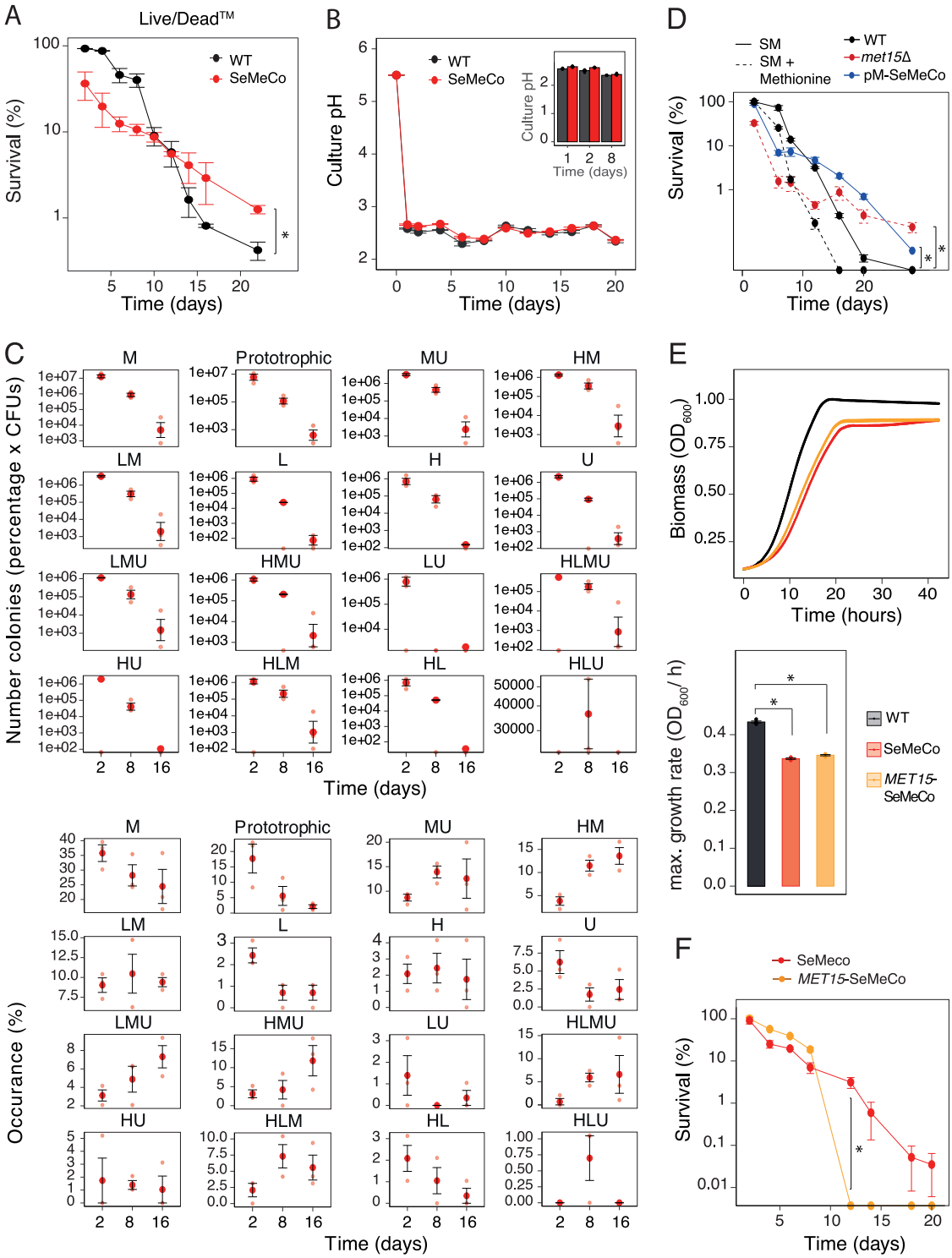

Figure S2. Metabolite exchange interactions extend lifespan in yeast communities, related to Figures 2 and 3

(A) Survival, as measured by staining of dead cells with the Live/Dead dye (see STAR Methods) of wild-type communities and SeMeCo. Data are mean ± SEM survival (percentage FC) compared with mean wild-type survival at the beginning of stationary phase; n = 3 biological replicates/strain. Statistics by unpaired two-sided t test; p values in Table S3.

(legend continued on next page)

(B) Culture pH values of chronologically aging wild-type communities and SeMeCo (same cultures as in Figure 2C). Data are mean ± SEM pH values per strain; n = 4 biological replicates/strain. Insets are culture pH values during exponential (1 day), early stationary (2 days), and stationary (8 days) growth phases; individual dots represent independent cultures. Statistics by unpaired two-sided Wilcoxon rank-sum test; p values in Table S7.

(C) Frequency of each metabotype (letters represent auxotrophy by plasmid segregation) in SeMeCo during CLS as (top) number of colonies, as calculated by the percentage of segregant cells from CFUs, and (bottom) percentage of segregant cells (see STAR Methods). Graphs show the mean ± SEM of n =3 biological replicates (smaller dots represent independent cultures). Statistics of pairwise comparison of each metabotype across CLS time points, by paired two-sided t test; p values in Table S4.

(D) CLS, as measured by HTP-CFU, of methionine auxotrophs (*met15Δ*) compared with wild-type yeast cultured in SM supplemented with 20 mg/L methionine (standard culture concentration) and single-plasmid SeMeCo (pM-SeMeCo) compared with wild-type cultured in SM medium (see STAR Methods). Data are mean ± SEM of n = 4 biological replicates/strain/culture media condition, shown as survival (percentage FC) compared with respective mean wild-type survival at the beginning of stationary phase. Statistics by unpaired two-sided Wilcoxon rank-sum test; p values in Table S3.

(E) (Top) Growth curves and (bottom) maximum growth, as measured by OD_{600nm}, of wild-type communities, SeMeCo, and *MET15*-SeMeCo grown on SM media. Data are mean ± SEM of n = 4 biological replicates/strain. Statistics by unpaired two-sided Wilcoxon rank-sum test; p value of wild type versus SeMeCo = 0.286 and wild type versus *MET15*-SeMeCo = 0.0286.

(F) CLS, as measured by HTP-CFU, of SeMeCo and *MET15*-SeMeCo. Data are mean ± SEM survival (percentage FC) compared with mean *MET15*-SeMeCo survival at the beginning of stationary phase; n = 3 biological replicates/strain. Statistics by unpaired one-sided Wilcoxon rank-sum test; p values in Table S3.

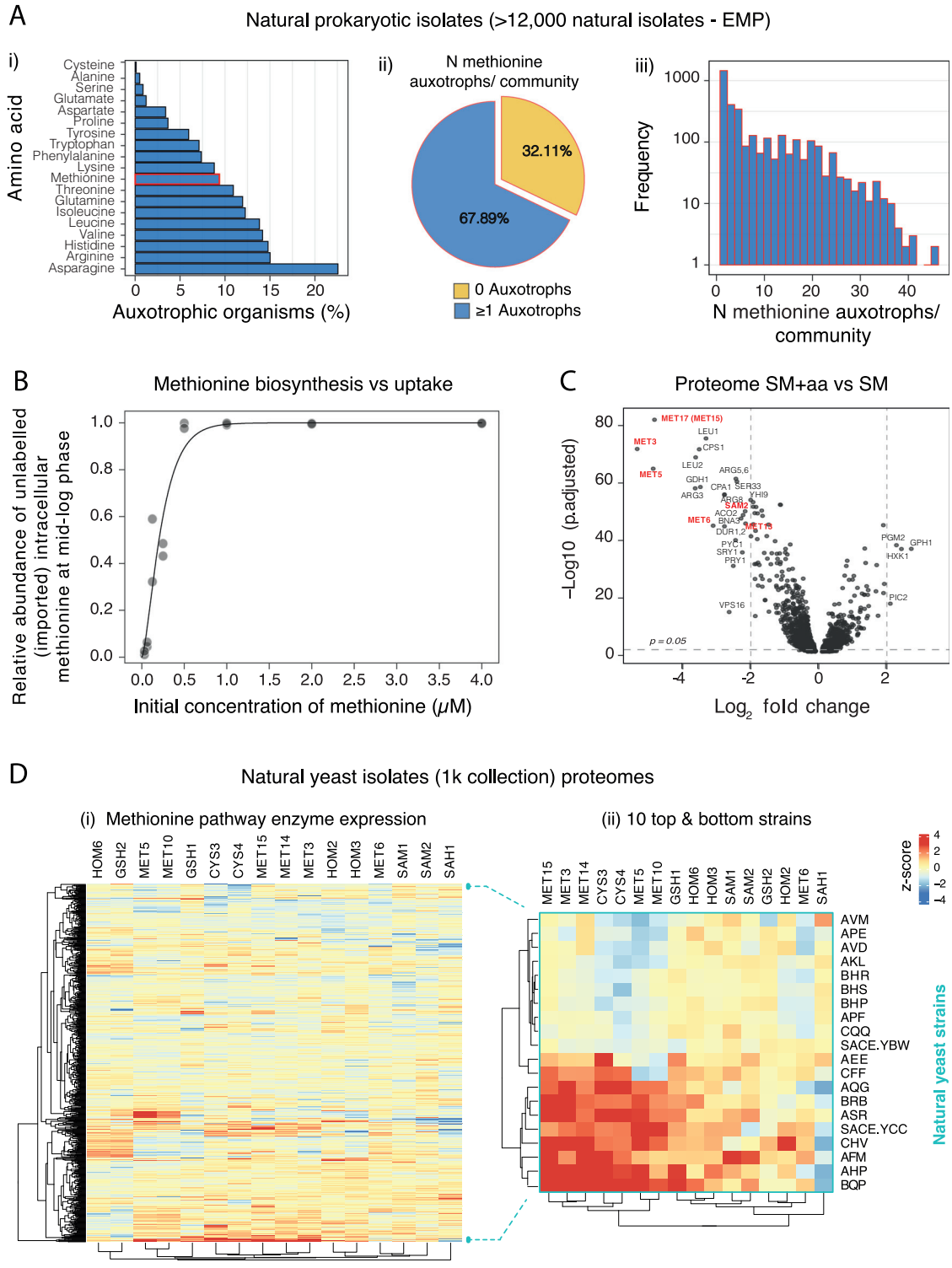

Figure S3. Methionine auxotrophy and methionine exchange is frequent in nature, related to Figure 3

(A) Frequency of methionine auxotrophic organisms in the bacterial and archaeal samples of the Earth Microbiome Project[53] collection, as analyzed by Machado et al. for the identification of amino acids auxotrophic species.[52] (i) Percentage of amino acid auxotrophic organisms (n total organisms = 5,559) in the analyzed EMP communities. (ii) Percentage of communities according to the number of methionine auxotrophic organisms per community. (iii) Frequency distribution of the number (N) of methionine auxotrophic organisms per community.

(legend continued on next page)

(B) Prototrophic wild-type yeast cells grown in SM media supplemented with 1% ^{13}C-glucose and unlabeled (^{12}C) methionine, at concentrations indicated on the x axis, were sampled at mid-log phase, for intracellular free amino acids analysis by HPLC-MS/MS[38] (see STAR Methods). Data shows the relative abundance of unlabeled (^{12}C, consumed) methionine compared with labeled (^{13}C, produced downstream of glucose catabolism) methionine (y axis). A cumulative gamma distribution was fitted to the data for visualization. Individual fraction values in Table S2.

(C) Proteome analysis of the prototrophic wild-type yeast strain cultured in the absence or presence of amino acid supplementation, SM or SM + aa, respectively (see STAR Methods). Volcano plot showing $\log_2$ expression fold change (FC) of SM + aa compared with SM cells. Horizontal dashed line indicates a threshold of adjusted p value significance of 0.05; vertical dashed lines indicate an absolute $\log_2$ FC of 2. Proteins indicated with red labels belong to the methionine biosynthetic pathway. Statistics by moderated two-sided t test and multiple testing correction with BH method, adjusted p values in Table S5.

(D) High-throughput untargeted proteomics analysis of the 1k yeast natural isolates collection.[55] Data is a re-analysis of the proteome dataset published by Muenzner et al.[54] (i) Heatmap showing broad heterogeneity in the expression levels of sulfur amino acids biosynthetic pathway. Data are *Z* score values, where red and blue show increased and decreased expression, respectively, relative to median expression per enzyme (columns) across natural yeast strains (rows). (ii) Zoom-in heatmap of the 10 top (extreme bottom) and 10 bottom (extreme top) strains clustering according to high and low enzyme expression, respectively.

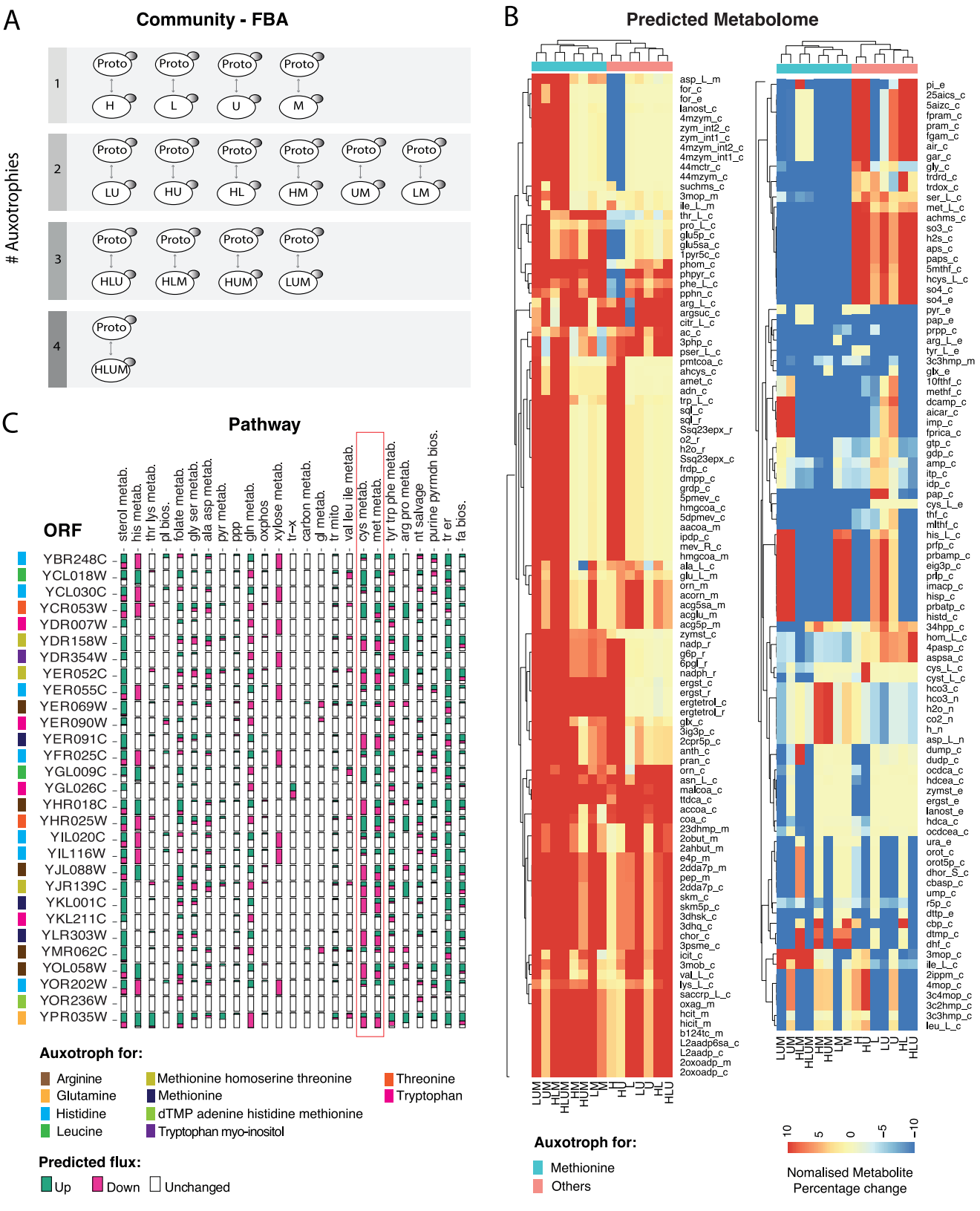

(legend on next page)

Figure S4. Genome-scale metabolic modeling predicts specific metabolome changes in communities where *MET15* and *met15Δ* cells interact, related to Figure 3

(A) Genome-scale metabolic modeling, using flux balance analysis (FBA), on pairwise communities of a prototroph (wild type) and each of the possible auxotrophs in a SeMeCo, in a total of 15 community pairs analyzed from Yu et al.[22]

(B) Heatmap showing predicted metabolite clustering according to when prototrophs in a community interact with methionine auxotrophs (unsupervised clustering). Columns are each prototroph-auxotroph community (auxotrophic label shown) and rows are predicted metabolites, represented in a −10 to 10 scale, where absolute percentage metabolite changes in auxotrophs versus prototroph >10% are scaled to 10 or −10 according to the directionality of change, as increased or decreased, respectively. The heatmap was split for visualization. Full list of metabolite names is in Table S1.

(C) Proportion of increased or decreased fluxes (>10%) in metabolic pathways (columns), upon the change from synthesis to uptake in different amino acid biosynthetic pathways, using FBA analysis. Modeled are genes (ORFs in rows) in which an auxotrophy can be introduced by a single-locus deletion (some amino acid auxotrophs would require multiple-locus deletion, see STAR Methods). Bios, biosynthesis; fa, fatty acid; metab, metabolism; nt, nucleotide; oxphos, oxidative phosphorylation; pl, phospholipid; ppp, pentose phosphate pathway; pyrmdn, pyrimidine; pyr, pyruvate; tca, tricarboxylic acid cycle; tr er, transport-endoplasmic reticulum; tr mito, transport-mitochondria; tr-n, transport-nuclear; tr-x, transport-peroxisomal. See Table S1.

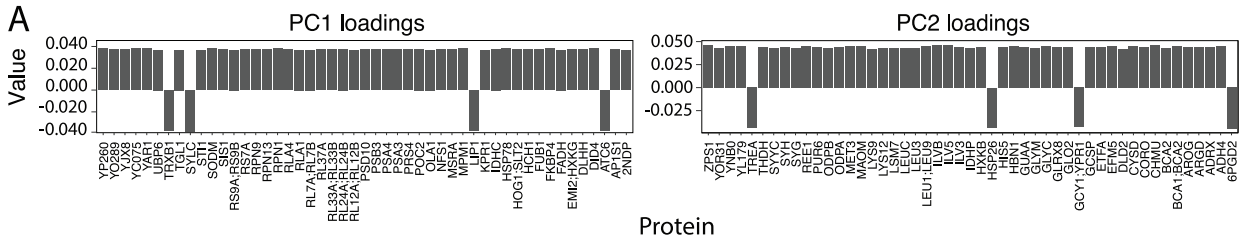

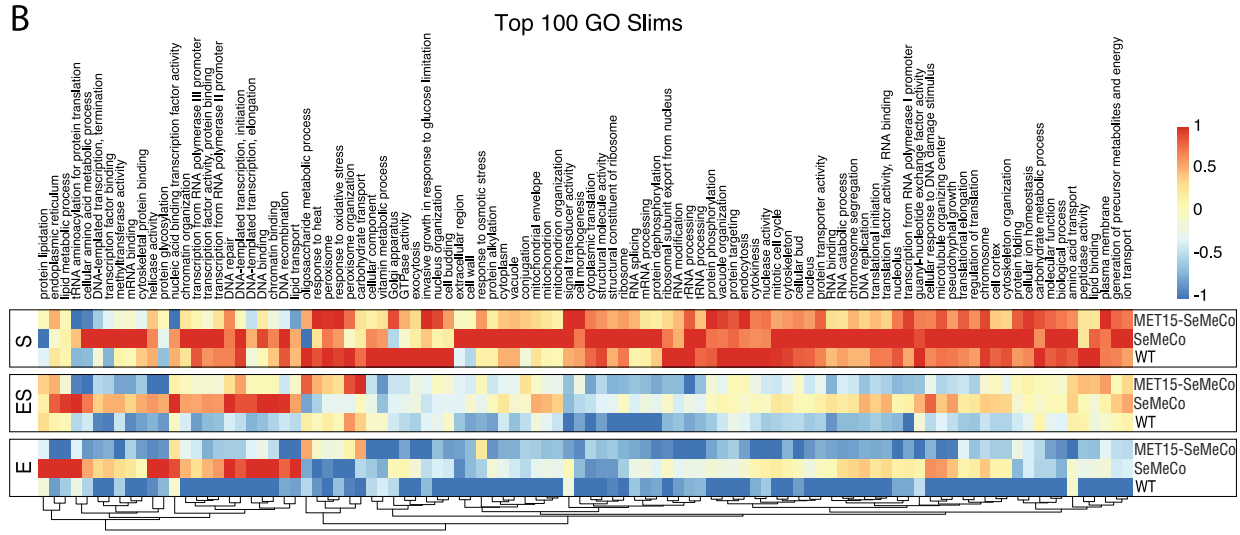

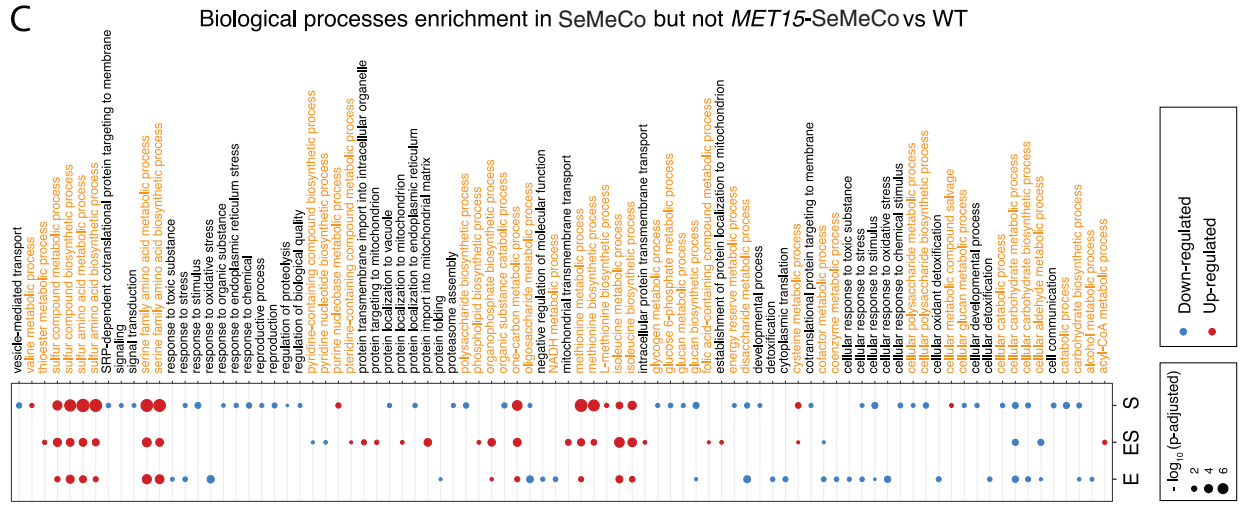

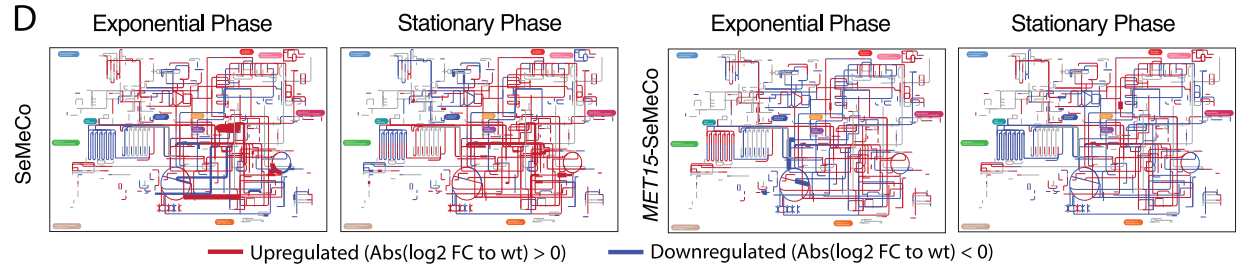

(legend on next page)

Figure S5. Proteome changes highlight metabolic adaptations in yeast communities where *MET15* and *met15⊿* cells interact, related to Figure 4

(A) Top 50 loadings from PCA1 and PCA2 mostly comprising proteins associated with growth phase and metabolic changes, respectively. Analysis derived from PCA analysis in Figure 4B.

(B) Heatmap showing mean expression of proteins, normalized to a −1 to 1 scale, belonging to top 100 GO slim terms (columns), per growth phase and yeast communities (rows).

(C) Gene ontology (GO) enrichment analysis showing significantly enriched (BH adjusted p value cutoff < 0.05) GO slim terms comprising biological processes in SeMeCo, but not in *MET15*-SeMeCo, compared with wild-type (WT) communities, during exponential (E), early stationary (ES), and stationary (S) growth phases.

(D) Differential metabolic enzyme expression levels mapped to the yeast metabolic network using iPath3[60] in exponential and stationary phases. Red and blue lines represent significantly (BH adjusted p value < 0.05) upregulated or downregulated proteins in SeMeCo and *MET15*-SeMeCo when compared with wild type; gray lines represent non-mapped/absent proteins in the measured proteomes. Thickness of the lines represent absolute $\log_2$ fold change (Abs($\log_2$FC)) changes (thickening = increased Abs($\log_2$FC)).

Data derived from proteome analysis in Figure 4A. Statistics by unpaired two-sided t test and multiple testing correction using the BH method; adjusted p values in Table S5.

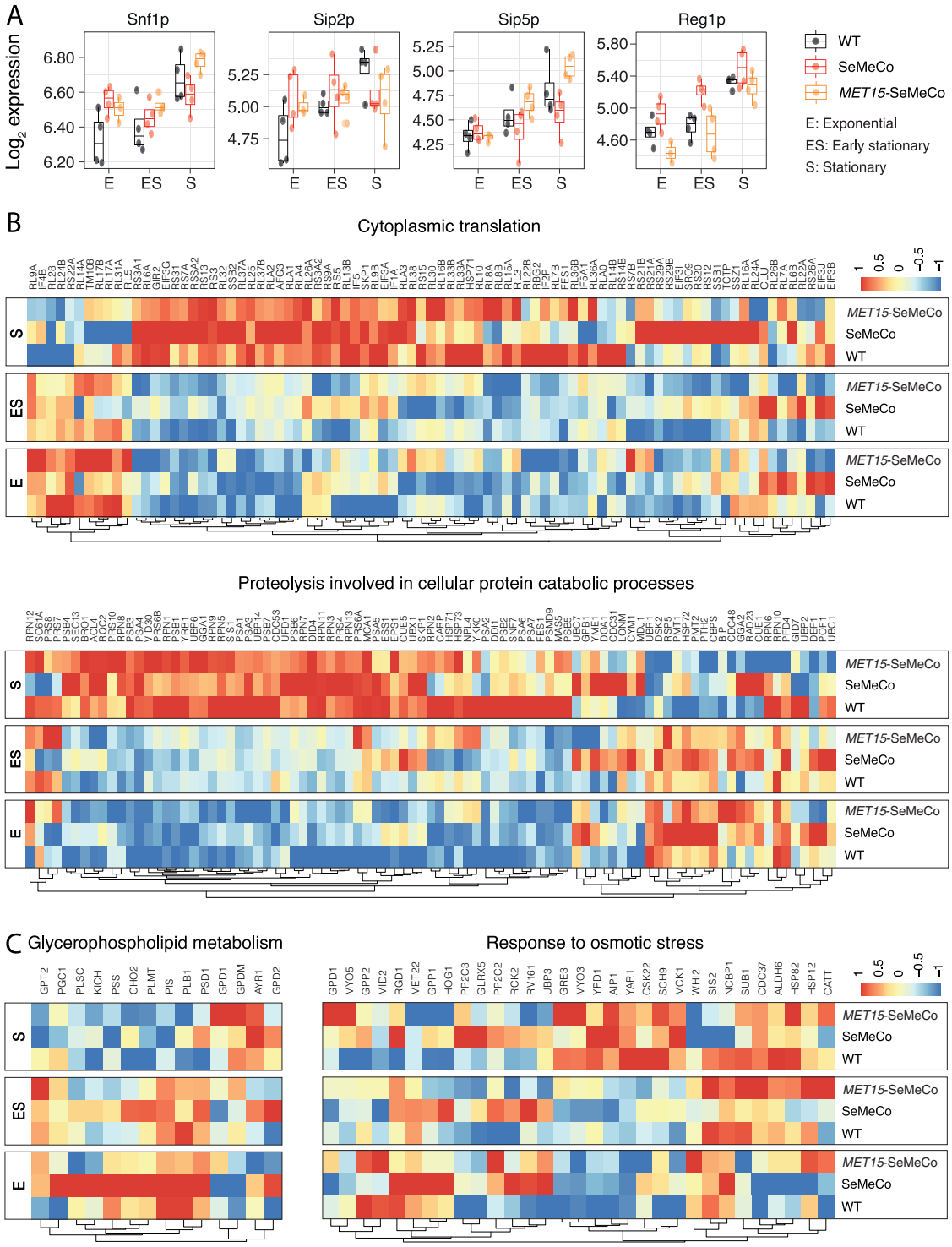

Figure S6. Methionine exchange interactions impact multiple biochemical processes of ageing, related to Figure 6

(A) Boxplots showing $\log_2$ expression of Snf1p and associated proteins. Boxplots represent median (50% quantile, middle line) and lower and upper quantiles (lower [25% quantile] and upper [75% quantile]). Dots represent values for individual biological replicates; n = 4 biological replicates/strain.

(B) Heatmaps showing expression of proteins (UniProt protein name, columns) belonging to the GO slim terms: "cytoplasmic translation" and "proteolysis involved in cellular protein catabolic processes," as a readout of TOR activity, per growth phase and yeast communities (rows).

(legend continued on next page)

(C) Heatmaps showing expression of protein (UniProt protein name, columns) belonging to the KEGG term: ''glycerophospholipid metabolism'' and to the GO slim term: ''response to osmotic stress,'' per growth phase and yeast communities (rows).
Data derived from proteome analysis in Figure 4A. Statistics by unpaired two-sided t test and multiple testing correction using the BH method; adjusted p value in Table S5. Data in heatmaps are the mean expression of n = 4 biological replicates/strain, normalized to a −1 to 1 scale.